**Supplementary Material**

# CoFeLDH for enhancement of Catalytic activity for the formation of Biologically active diaryl sulfide and propargylamine derivatives and studies on their biocidal activity including molecular docking and DFT studies for anti-diabetic activity

Aminul Islam[a], Rabindranath Singha[a], Susanta Kumar Saha[b], Kaushik Sarkar[a], Tania Baishya[c], Ranabir Sahu[c], Rajesh Kumar Das[a], Malay Bhattacharya[d], Mayukh Deb[a] and Pranab Ghosh[a]*

[a]*Department of Chemistry, University of North Bengal, Dist-Darjeeling, West Bengal, India*

[b]*Department of Engineering Sciences and Humanities, Siliguri Institute of Technology, Darjeeling, 734009, West Bengal, India*

[c]*Department of Pharmaceutical Technology, North Bengal University, Darjeeling 734 013, West Bengal, India*

[d]*Department of Tea Science, North Bengal University, Darjeeling 734 013, West Bengal, India*

E-mail address: pizy12@yahoo.com (P.Ghosh)

**Table of contents**



## 1. General information

The experiment confidently utilized reagents from highly reputable commercial suppliers such as Sigma-Aldrich, TCI, and AlfaAesar, without requiring any additional purification. Solvents from commercial suppliers were also utilized after thorough distillation. The synthesized products underwent successful purification via column chromatography utilizing 60-120 mesh silica gels from SRL, India. Thin Layer Chromatography (TLC) was conducted using Merck plates coated with silica gel 60, $F_{254}$, which proved to be highly effective. The $^{1}H$ & $^{13}C$ NMR analyses were confidently

conducted using a 400 MHz BrukerAvance FT-NMR Spectrometer, with TMS serving as a reliable and consistent internal standard.

**2. General procedure for the Synthesis of the Diaryl Sulfide Derivatives:**

For this particular experiment, a round-bottom flask with a volume of 25 mL was filled with 1 mmol of 4-iodoanisole, 1 mmol of thiophenol, and 1.3 mmol of $K_2CO_3$ in DMF medium. CoFeLDH weighing 25 mg was also added to the flask, which was then heated under reflux conditions. The reaction mixture was stirred until the reactants were depleted, as shown by TLC. Once the reaction had ended, the catalyst was removed by simple filtration, and the organic portion of the reaction was separated using a separating funnel with a straightforward workup process. The final products were then purified by column chromatography, utilizing 60-120 mesh silica gels.

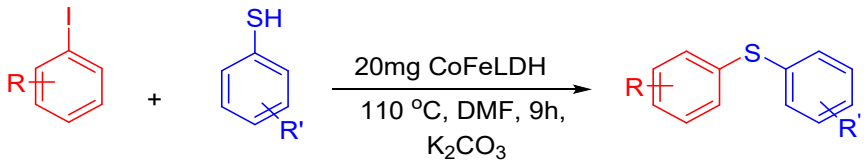


**Scheme 1:** Synthetic procedure for Diaryl Sulfide Derivatives

**3. General procedure for the Synthesis of the Propargylamine Derivatives:**

In this experiment, a 25 mL round-bottom flask was filled with a mixture of benzaldehyde (1 mmol), phenylacetylene (1 mmol), and morpholine (1 mmol). To this mixture, 25 mg of CoFeLDH catalyst was added in DMF (reaction medium) and heated under reflux conditions. The reaction mixture was stirred under reflux conditions until the reactants were completely consumed, as indicated by TLC. After the reaction was complete, the catalyst was separated by simple filtration, and the organic part of the reaction was separated using a separating funnel with a simple workup. Finally, the products were purified by column chromatography on 60-120 mesh silica gels.

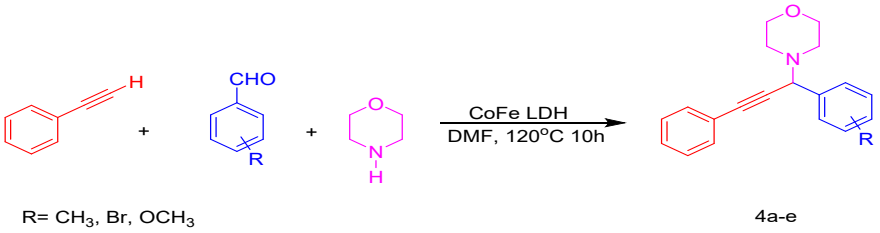


**Scheme 2:** Synthetic procedure for propargylamine derivatives

**4. Characterization of products:**

**1. (2-Methoxyphenyl)(phenyl)sulfane (3a)[19]**

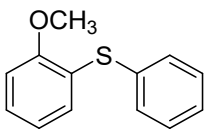


Colourless oil; IR (neat) $\nu_{max}$: 2974, 2837, 753, 690 $cm^{-1}$; $^1H$ NMR (400 MHz, $CDCl_3$): δ = 7.23-7.38 (m, 6 H), 7.09-7.12 (m, 1H), 6.86-6.92 (m, 2 H), 3.87 (s, 3H);$^{13}C$ NMR (100 MHz, $CDCl_3$): δ = 157.36, 134.55, 132.96, 130.13, 129.18, 128.39, 126.90, 124.10, 121.29, 110.92, 55.92;

Elemental analysis: C% H% O% S%

Calculated: 72.19 5.59 7.40 14.82

Experimental: 71.86 5.68 7.20 13.93

2. **(3-Methoxyphenyl)(phenyl)sulfane (3b)[19]**

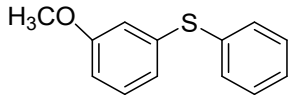

Pale yellow liquid, IR (neat) $\nu_{max}$: 3078, 3026, 2954, 2932, 2806, 691 $cm^{-1}$; $^{1}H$ NMR (400 MHz, $CDCl_3$): δ = 7.19-7.40 (m, 6), 6.87-6.93 (m, 2H), 6.74-6.77 (m, 1H), 3.71 (s, 3H); $^{13}C$ NMR (100 MHz, $CDCl_3$): δ = 160.07, 137.25, 135.29, 131.44, 129.96, 129.23, 127.27, 122.98, 115.93, 112.81, 55.28.

Elemental analysis: C% H% O% S%

Calculated: 72.19 5.59 7.40 14.82

Experimental: 71.86 5.68 7.20 14.98

3. **(4-Methoxyphenyl)(phenyl)sulfane (3c)[19]**

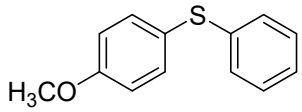

Pale yellow liquid, IR (neat) $\nu_{máx}$: 3088, 3042, 2942, 2918, 2802, 692 $cm^{-1}$.

$^{1}$HNMR ($CDCl_3$, 400MHz): δ = 7.42 (d, *J* = 8.8 Hz, 2H), 7.14-7.26 (m, 5H), 6.89-6.91 (m, 2H), 3.82 (s, 3H); $^{13}$CNMR (100 MHz, $CDCl_3$): δ = 159.84, 138.61, 135.38, 128.94, 128.22, 125.78, 124.33, 115.00, 55.38;

Elemental analysis: C% H% O% S%

Calculated: 72.19 5.59 7.40 14.82

Experimental: 71.86 5.68 7.20 13.93

4. **(4-chlorophenyl)(4-methoxyphenyl)sulfane (3d)[19]**

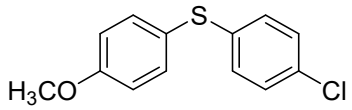

Colourless oil, IR (neat) $\nu_{máx}$: 2960, 2933, 1578, 1472, 1275, 741, 685 $cm^{-1}$;

$^{1}H$ NMR (400 MHz, $CDCl_3$): δ = 7.40-7.42 (m, 2H), 7.18-7.21 (m, 2H), 7.07-7.10 (m, 2H), 6.90-6.92 (m, 2H), 3.82 (s, 3H); $^{13}C$ NMR (100 MHz, $CDCl_3$): δ = 160.08,137.40, 135.89, 132.19, 131.61, 129.33, 129.03, 115.16, 55.39;

Elemental analysis: C% H% O% S% Cl%

Calculated: 62.27 4.42 6.38 12.79 14.14

Experimental: 61.99 5.02 6.15 13.05 14.50

**5**. **(2-Methoxyphenyl)(p-tolyl)sulfane (3e)[19]**

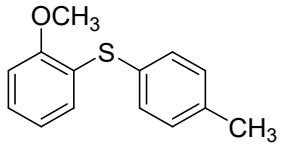

Colorless liquid, IR (neat) $\nu_{max}$: 3002, 2935, 2835, 1576, 1473, 1272, 743, 683 $cm^{-1}$;

$^1H$ NMR (400 MHz, $CDCl_3$): δ = 7.32 (d, *J* = 8.0 Hz, 2H), 7.15-7.25 (m, 3H), 6.81-6.96 (m, 3H), 3.89 (s, 3H), 2.36 (s, 3H); $^{13}C$ NMR (100 MHz, $CDCl_3$): δ = 156.54, 137.74, 132.97, 130.11, 129.91, 129.81, 127.44, 125.72, 121.22, 110.63, 55.89, 21.19;

Elemental analysis: C% H% O% S%

Calculated: 73.01 6.13 6.95 13.92

Experimental: 74.05 5.98 7.10 14.15

**6. (4-Chlorophenyl)(3-nitrophenyl)sulfane (3f)[19]**

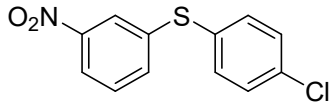

Yellow solid, m.p. 58 °C, IR (KBr) $\nu_{máx}$: 1573, 1506, 1337, 688 $cm^{-1}$;

$^1$HNMR ($CDCl_3$, 400MHz) δ= 8.07 (d, *J* = 8.4 Hz, 2H), 7.49-7.99 (m, 2H), 7.25-7.45;$^{13}$CNMR (100 MHz, $CDCl_3$), δ= 148.74, 139.80, 135.20, 134.53, 134.48, 130.90, 130.07, 129.88, 123.46, 121.33.

Elemental analysis: C% H% O% S% Cl% N%

Calculated: 54.24 3.03 12.04 12.07 13.34 5.27

Experimental: 53.98 3.20 11.95 12.23 13.53 4.98

7. **(4-Nitrophenyl)(p-tolyl)sulfane (3g)[19]**

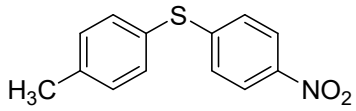

Yellow solid, m.p.: 87 °C; IR (KBr) $\nu_{máx}$: 1570, 1506, 1338, 686 $cm^{-1}$;

$^1H$ NMR (400 MHz, $CDCl_3$): δ = 8.06 (d, *J* = 8.4, 2H), 7.43 (d, *J* = 8.0, 2H), 7.26 (d, *J* = 7.6, 2H), 7.15 (d, *J* = 8.4, 2H), 2.41 (s, 3H); $^{13}C$ NMR (100 MHz, $CDCl_3$): δ = 149.35,145.14, 140.25, 135.09, 130.87, 126.49, 126.13, 123.98, 21.35;

Elemental analysis: C% H% O% S% N%

Calculated: 63.65 4.52 13.04 13.07 5.71

Experimental: 64.07 3.97 12.95 13.23 5.98

8. **1-(4-(p-Tolylthio)phenyl)ethanone (3h)[19]**

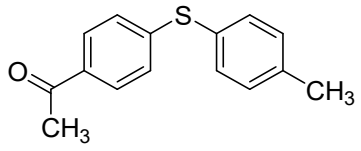

White solid, m.p.: 93°C, IR (KBr) $\nu_{máx}$: 3059, 3009, 2943, 2915, 2821, 1685, 680 $cm^{-1}$;$^1H$ NMR (400 MHz, $CDCl_3$): δ = 7.77-7.80 (m, 2H), 7.39-7.42 ( d, *J* = 8.1 Hz, 2H ), 7.21-7.25 (m, 2H), 7.13-7.16

(m, 2H), 2.53 (s, 3H), 2.39 (s, 3H); $^{13}$C NMR (100 MHz, $CDCl_3$): δ = 197.18, 145.96, 139.35, 134.50, 134.14, 130.53, 128.83, 127.91, 126.66, 26.44, 21.28;

| Elemental analysis: | C% | H% | O% | S% |
|---|---|---|---|---|
| Calculated: | 74.35 | 5.82 | 6.60 | 13.23 |
| Experimental: | 44.75 | 6.10 | 6.95 | 13.40 |

**9. 4-(1,3-diphenylprop-2-ynyl)morpholine (4a)[36]**

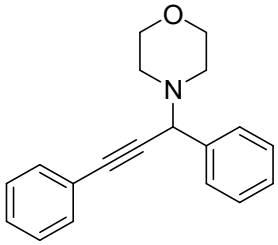


Brown oil; Yield 95%; $^1$H NMR ( 400 MHz, $CDCl_3$ ): δ = 7.53-7.69 (m, 2H), 7.47-7.49 (m, 2H), 7.25-7.42 (m, 6H), 4.83 (s, 1H), 3.76 (s, 4H), 2.67 (s, 4H); $^{13}$ C NMR (100 MHz, $CDCl_3$): δ = 137.79, 132.49, 131.86, 129.94, 128.36, 127.85, 127.22, 127.15, 123.01, 88.57,85.09, 66.92, 62.07, 49.91, 29.40.

| Elemental analysis: | C% | H% | N% | O% |
|---|---|---|---|---|
| Calculated: | 82.28 | 6.90 | 5. 05 | 5.77 |
| Experimental: | 81.98 | 7.10 | 5.43 | 5.20 |

**10. 4-(3-phenyl-1-p-tolylprop-2-ynyl)morpholine (4b)[36]**

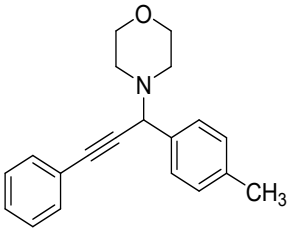


$^1$H NMR (400 MHz, $CDCl_3$): δ = 7.52-7.54 (m, 4H), 7.32-7.36 (m, 3H), 7.19-7.25 (m, 2H), 4.77 (s, 1H), 3.70-3.79 (s, 4H), 2.60-2.69 (s, 4H), 2.38(s, 3H); $^{13}$ C NMR (100 MHz, $CDCl_3$): δ = 137.52, 134.82, 131.84, 128.97, 128.56, 128.34, 128.25, 123.07, 88.29, 85.37, 67.20, 61.82, 49.91, 21.18.

| Elemental analysis: | C% | H% | N% | O% |
|---|---|---|---|---|
| Calculated: | 82.44 | 7. 6 | 4.81 | 5.49 |
| Experimental: | 83.05 | 7.44 | 5.06 | 5.20 |

**11. 4-(1-(4-methoxyphenyl)-3-phenylprop-2-ynyl)morpholine (4c)[36]**

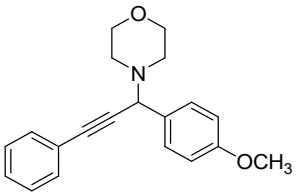

$^{1}$H NMR ( 400 MHz, $CDCl_3$ ): δ = 7.49-7.56 (m, 4H), 7.31-7.34 (m, 2H), 6.88-6.92 (m, 2H), 4.74 (s, 1H), 3.81 (m, 3H), 3.70-3.78 (m, 4H), 2.59-2.67 (m, 4H);$^{13}$ C- NMR (100 MHz, $CDCl_3$): δ = 159.23, 131.81, 129.77, 128.32, 128.25, 123.02, 114.44, 113.58, 88.29, 85.37, 67.14, 61.46, 55.30, 49.81.

| Elemental analysis: | C% | H% | N% | O% |
|---|---|---|---|---|
| Calculated: | 78.15 | 6.89 | 4.56 | 10.41 |
| Experimental: | 78.30 | 6.65 | 4.93 | 10.05 |

**12. 4-(3-phenyl-1-o-tolylprop-2-ynyl)morpholine (4d)[36]**

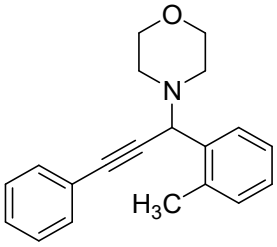


$^{1}$H NMR (400 MHz, $CDCl_3$): δ = 7.76 (s, 1H), 7.57-7.59 (m, 2H), 7.37-7.40 (m, 3H), 7.26-7.28 (m, 3H), 4.93 (s, 1H), 3.70-3.78 (m, 4H), 2.69 (s, 4H), 2.54 ( s, 3H);$^{13}$ C- NMR (100 MHz, $CDCl_3$): δ = 137.58, 135.84, 131.87, 130.80, 130.10, 129.10, 128.28, 125.45, 123.16, 88.69, 85.12, 67.29, 59.90, 49.78, 19.18.

| Elemental analysis: | C% | H% | N% | O% |
|---|---|---|---|---|
| Calculated: | 82.44 | 7. 6 | 4.81 | 5.49 |
| Experimental: | 83.05 | 7.44 | 5.06 | 5.20 |

**13. 4-(1-(2-bromophenyl)-3-phenylprop-2-ynyl)morpholine (4e)[36]**

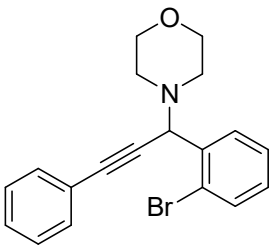


$^{1}$H NMR (400 MHz, $CDCl_3$): δ = 7.52-7.55 (m, 1H), 7.25-7.37 (m, 3H), 7.15-7.20 (m, 5H), 5.11 (s, 1H), 3.67-3.78 9 (m, 4), 2.66-2.75 (m, 4H); $^{13}$ C NMR (100 MHz, $CDCl_3$): δ = 137.19, 133.35, 131.88, 130.72, 129.47, 128.43, 127.02, 125.34, 122.83, 88.75, 84.67, 67.14, 61.38, 49.77.

| Elemental analysis: | C% | H% | N% | O% | Br% |
|---|---|---|---|---|---|
| Calculated: | 64.06 | 5.09 | 3.93 | 4.49 | 22.43 |
| Experimental: | 64.43 | 4.98 | 4.05 | 4.68 | 22.15 |

**5. Copies of NMR Spectra:**

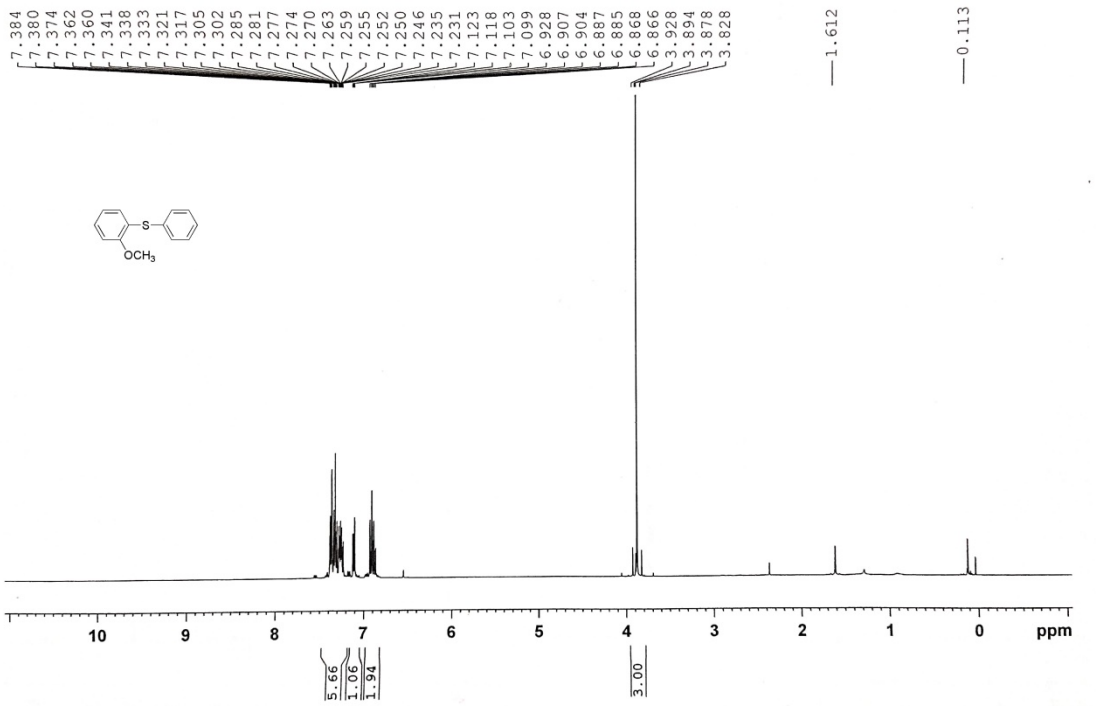
7.384
7.380
7.374
7.362
7.360
7.341
7.338
7.333
7.321
7.317
7.305
7.302
7.285
7.281
7.277
7.274
7.270
7.263
7.259
7.255
7.252
7.250
7.246
7.235
7.231
7.123
7.118
7.103
7.099
6.928
6.907
6.904
6.887
6.885
6.868
6.866
3.928
3.894
3.878
3.828
1.612
0.113
S
OCH3
10
9
8
7
6
5
4
3
2
1
0
ppm
5.66
1.06
1.94
3.00

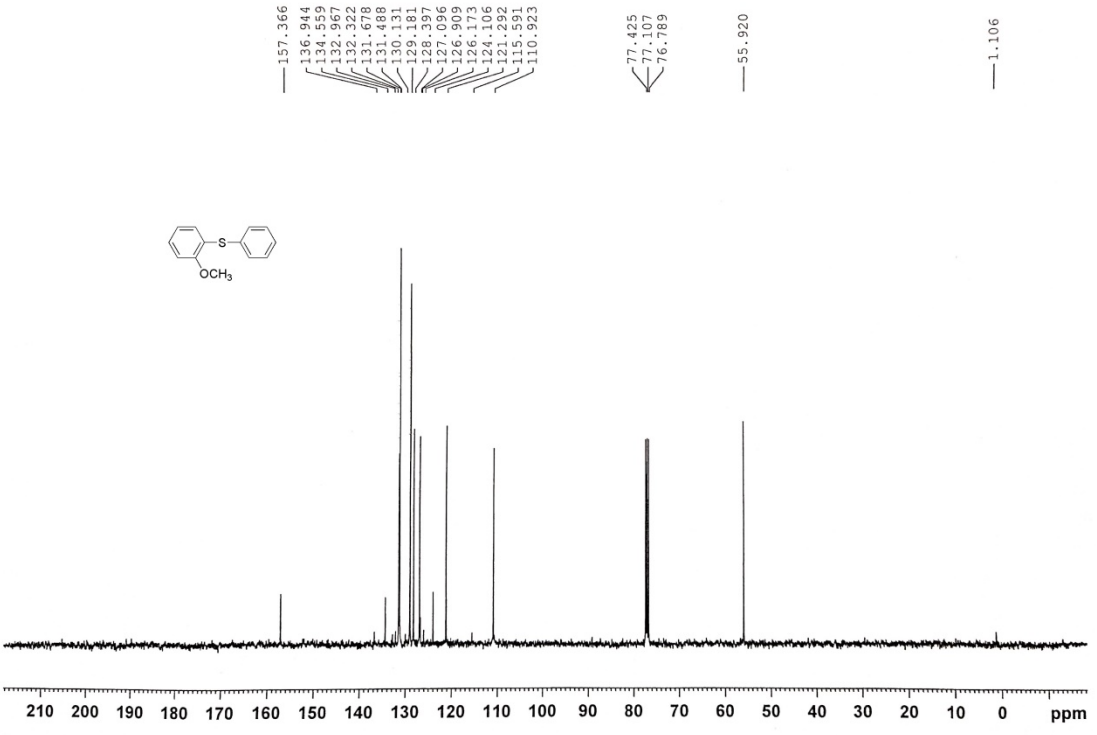
157.366
136.944
134.559
132.967
132.322
131.678
131.488
130.131
129.181
128.397
127.096
126.909
126.173
124.106
121.292
115.591
110.923
77.425
77.107
76.789
55.920
1.106
S
OCH3
210
200
190
180
170
160
150
140
130
120
110
100
90
80
70
60
50
40
30
20
10
0
ppm

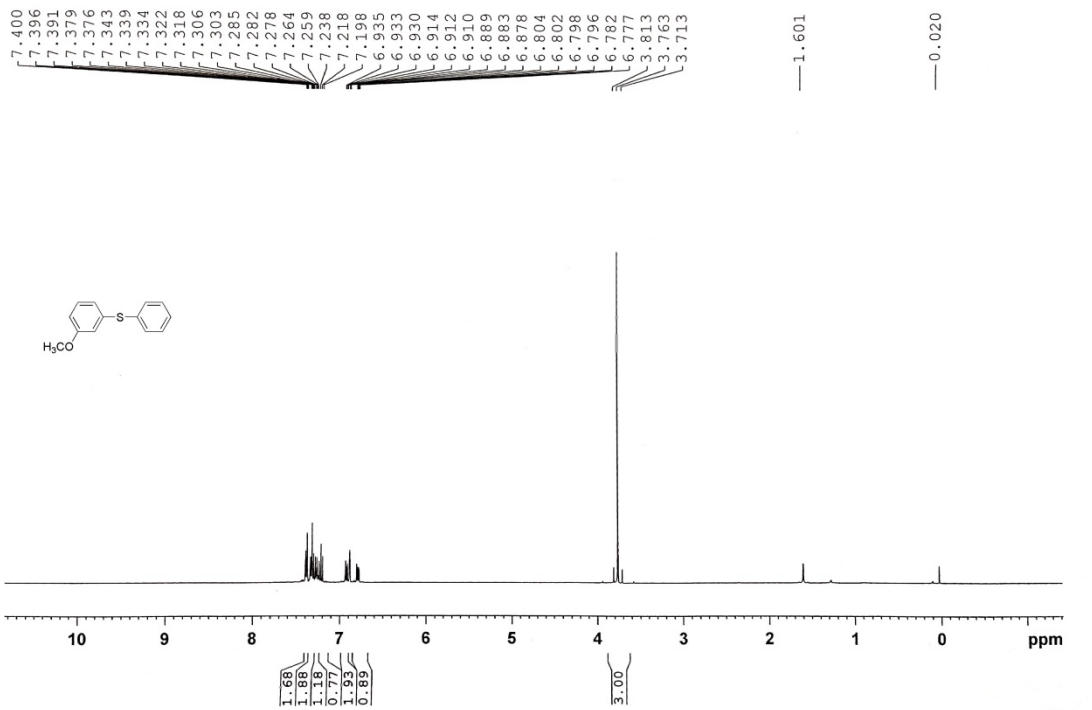
7.400
7.396
7.391
7.379
7.376
7.343
7.339
7.334
7.322
7.318
7.306
7.303
7.285
7.282
7.278
7.264
7.259
7.238
7.218
7.198
6.935
6.933
6.930
6.914
6.912
6.910
6.889
6.883
6.878
6.804
6.802
6.798
6.796
6.782
6.777
3.813
3.763
3.713
1.601
0.020
H3CO
10
9
8
7
6
5
4
3
2
1
0
ppm
1.68
1.88
1.18
0.77
1.93
0.89
3.00

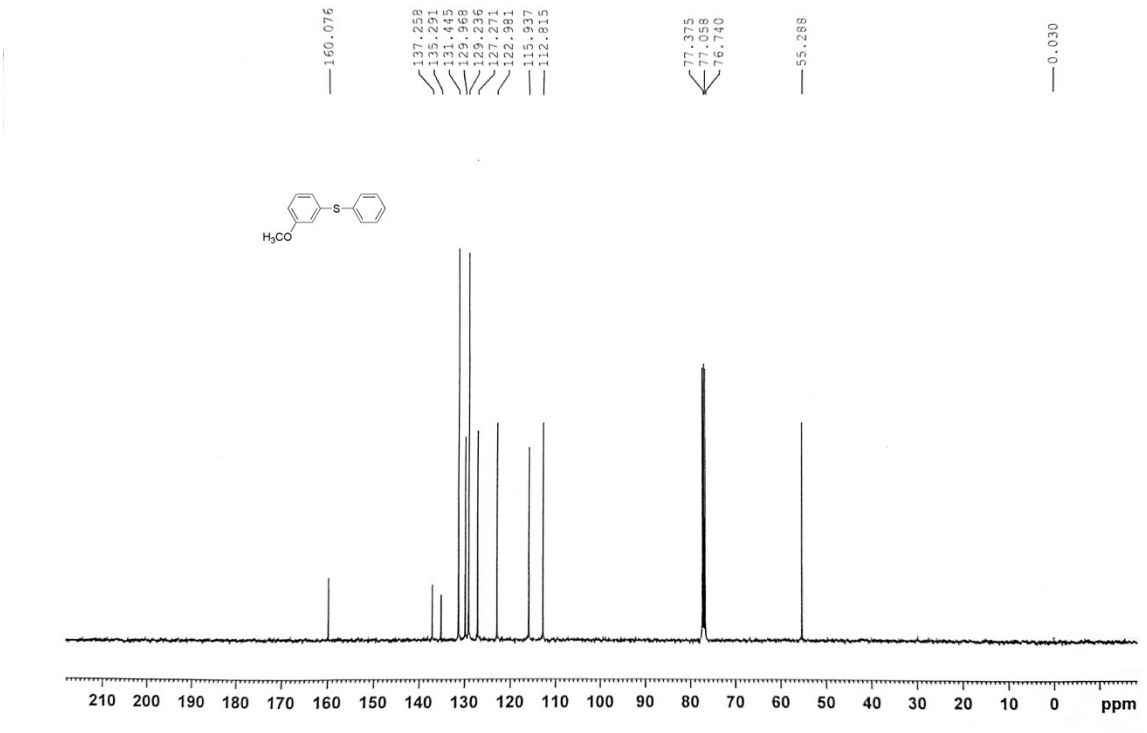
160.076
137.258
135.291
131.445
129.968
129.236
127.271
122.981
115.937
112.815
77.375
77.058
76.740
55.288
0.030
H3CO
210
200
190
180
170
160
150
140
130
120
110
100
90
80
70
60
50
40
30
20
10
0
ppm

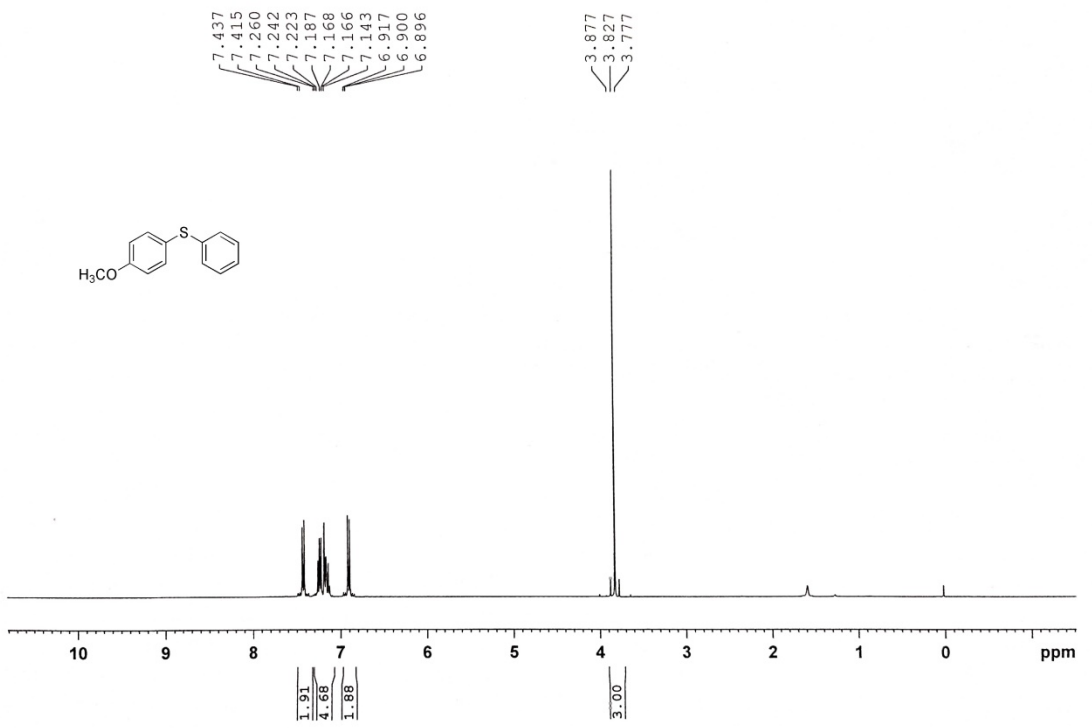
7.437
7.415
7.260
7.242
7.223
7.187
7.168
7.166
7.143
6.917
6.900
6.896
3.877
3.827
3.777
H3CO
S
10
9
8
7
6
5
4
3
2
1
0
ppm
1.91
4.68
1.88
3.00

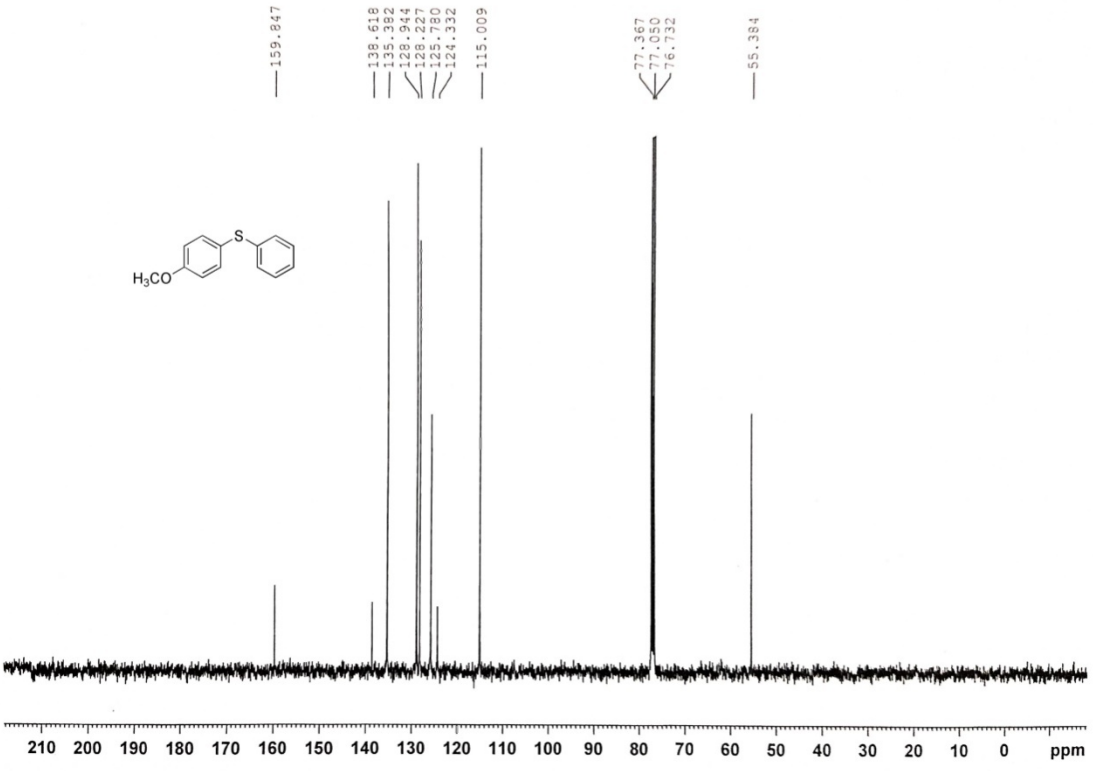
159.847
138.618
135.382
128.944
128.227
125.780
124.332
115.009
77.367
77.050
76.732
55.384
H3CO
S
210
200
190
180
170
160
150
140
130
120
110
100
90
80
70
60
50
40
30
20
10
0
ppm

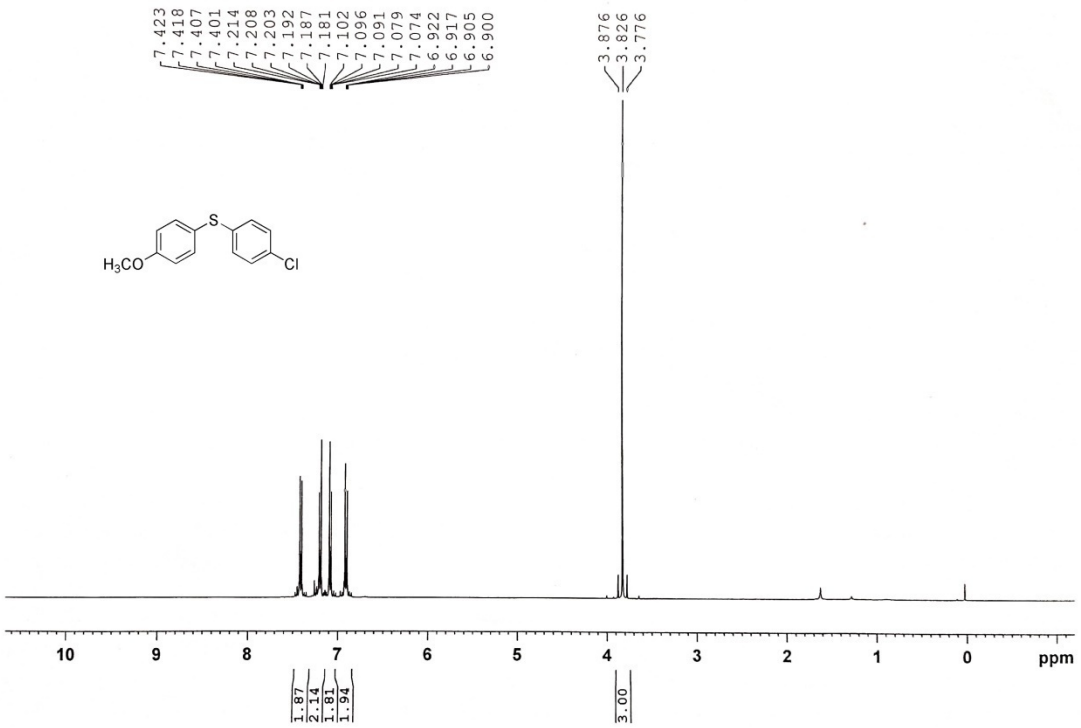
7.423
7.418
7.407
7.401
7.214
7.208
7.203
7.192
7.187
7.181
7.102
7.096
7.091
7.079
7.074
6.922
6.917
6.905
6.900
3.876
3.826
3.776
H3CO
S
Cl
10
9
8
7
6
5
4
3
2
1
0
ppm
1.87
2.14
1.81
1.94
3.00

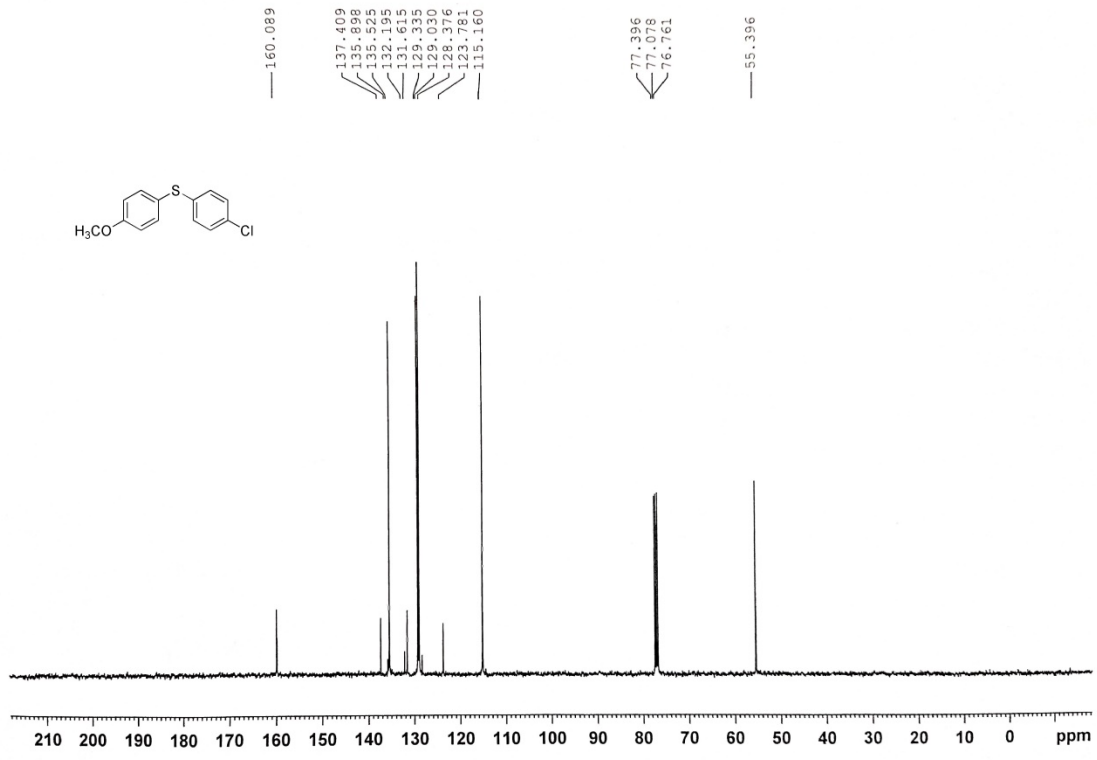
160.089
137.409
135.898
135.525
132.195
131.615
129.335
129.030
128.376
123.781
115.160
77.396
77.078
76.761
55.396
H3CO
S
Cl
210
200
190
180
170
160
150
140
130
120
110
100
90
80
70
60
50
40
30
20
10
0
ppm

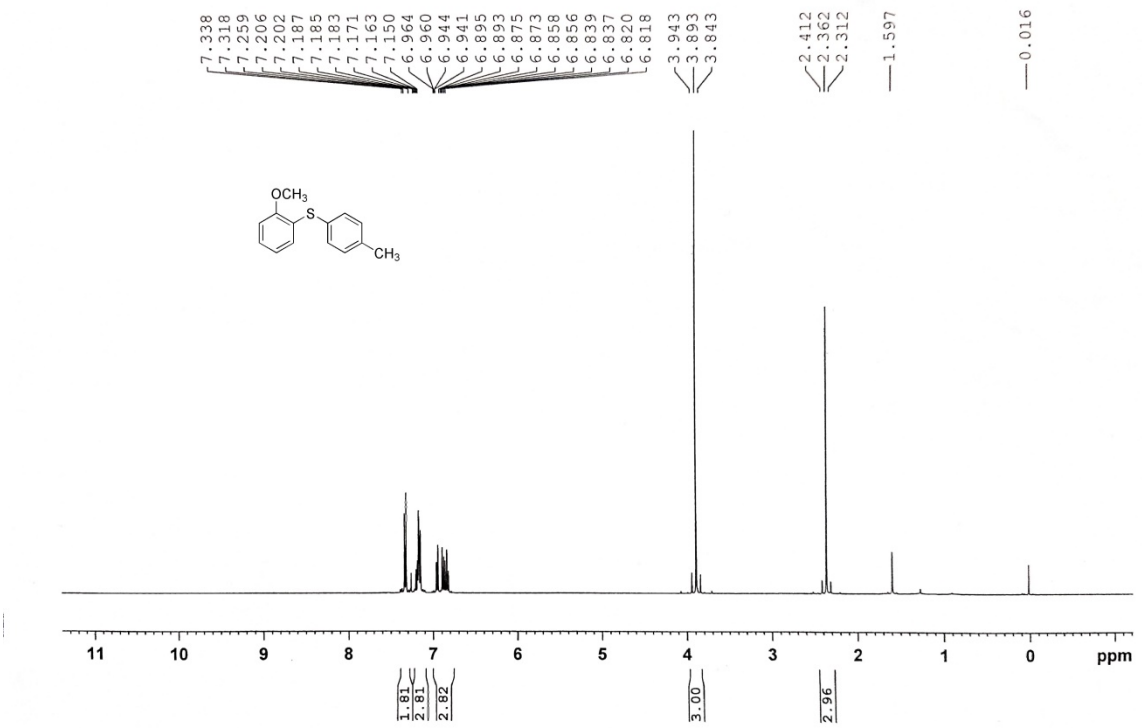
7.338
7.318
7.259
7.206
7.202
7.187
7.185
7.183
7.171
7.163
7.150
6.964
6.960
6.944
6.941
6.895
6.893
6.875
6.873
6.858
6.856
6.839
6.837
6.820
6.818
3.943
3.893
3.843
2.412
2.362
2.312
1.597
0.016
OCH3
S
CH3
11
10
9
8
7
6
5
4
3
2
1
0
ppm
1.81
2.81
2.82
3.00
2.96

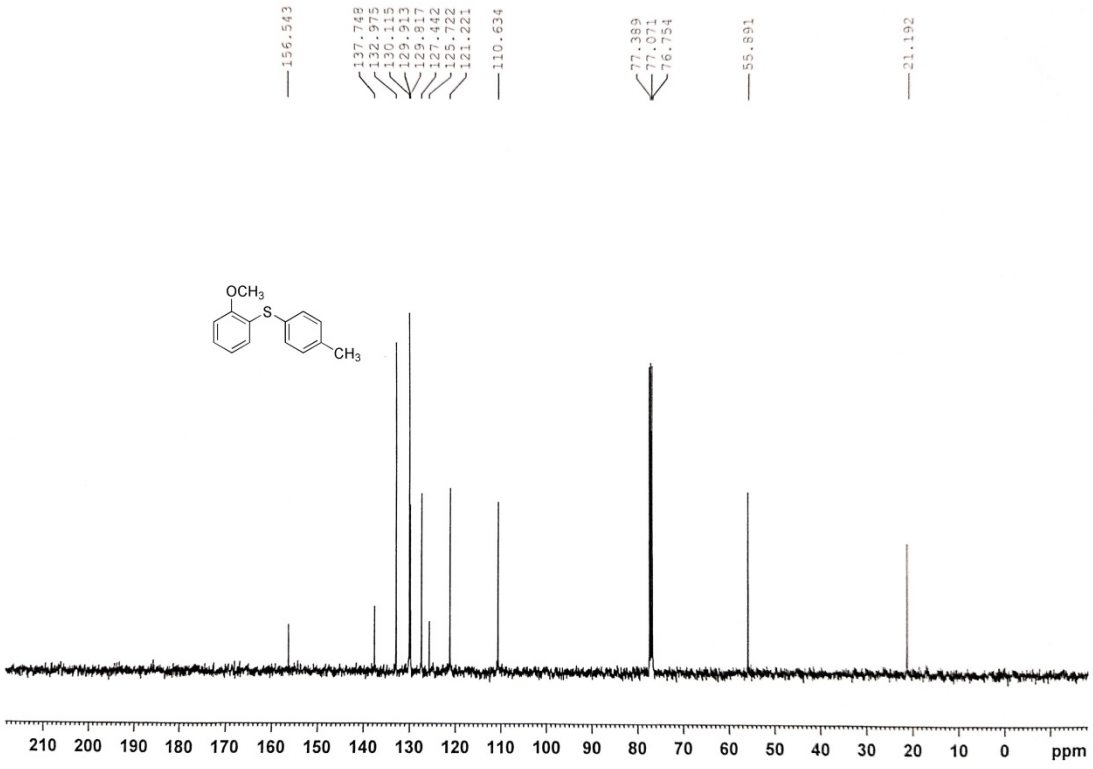
156.543
137.748
132.975
130.115
129.913
129.817
127.442
125.722
121.221
110.634
77.389
77.071
76.754
55.891
21.192
OCH3
S
CH3
210
200
190
180
170
160
150
140
130
120
110
100
90
80
70
60
50
40
30
20
10
0
ppm

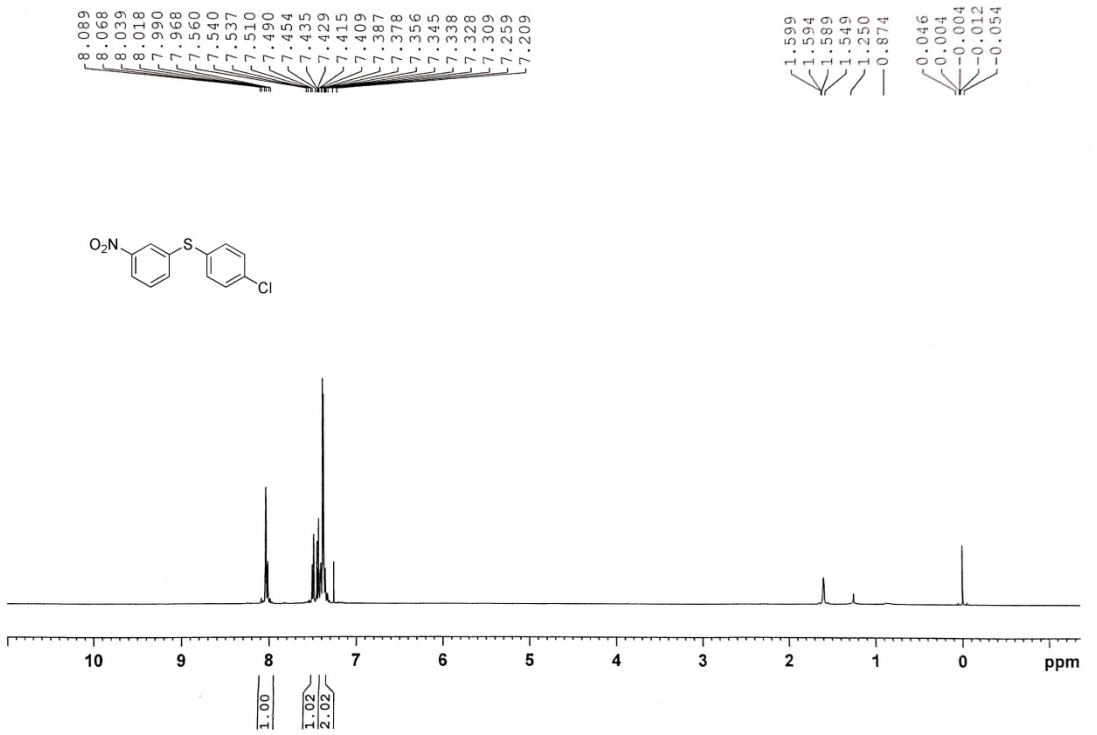
8.089
8.068
8.039
8.018
7.990
7.968
7.560
7.540
7.537
7.510
7.490
7.454
7.435
7.429
7.415
7.409
7.387
7.378
7.356
7.345
7.338
7.328
7.309
7.259
7.209
1.599
1.594
1.589
1.549
1.250
0.874
0.046
0.004
-0.004
-0.012
-0.054
O2N
S
Cl
10
9
8
7
6
5
4
3
2
1
0
ppm
1.00
1.02
2.02

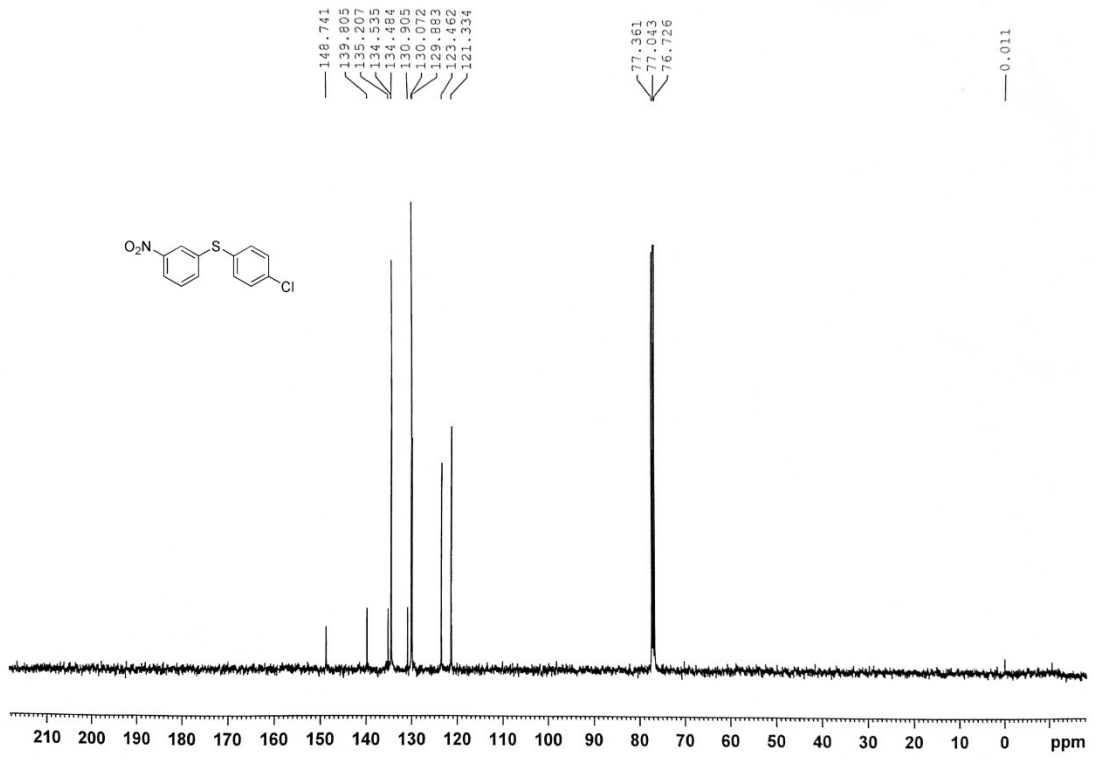
148.741
139.805
135.207
134.535
134.484
130.905
130.072
129.883
123.462
121.334
77.361
77.043
76.726
0.011
O2N
S
Cl
210
200
190
180
170
160
150
140
130
120
110
100
90
80
70
60
50
40
30
20
10
0
ppm

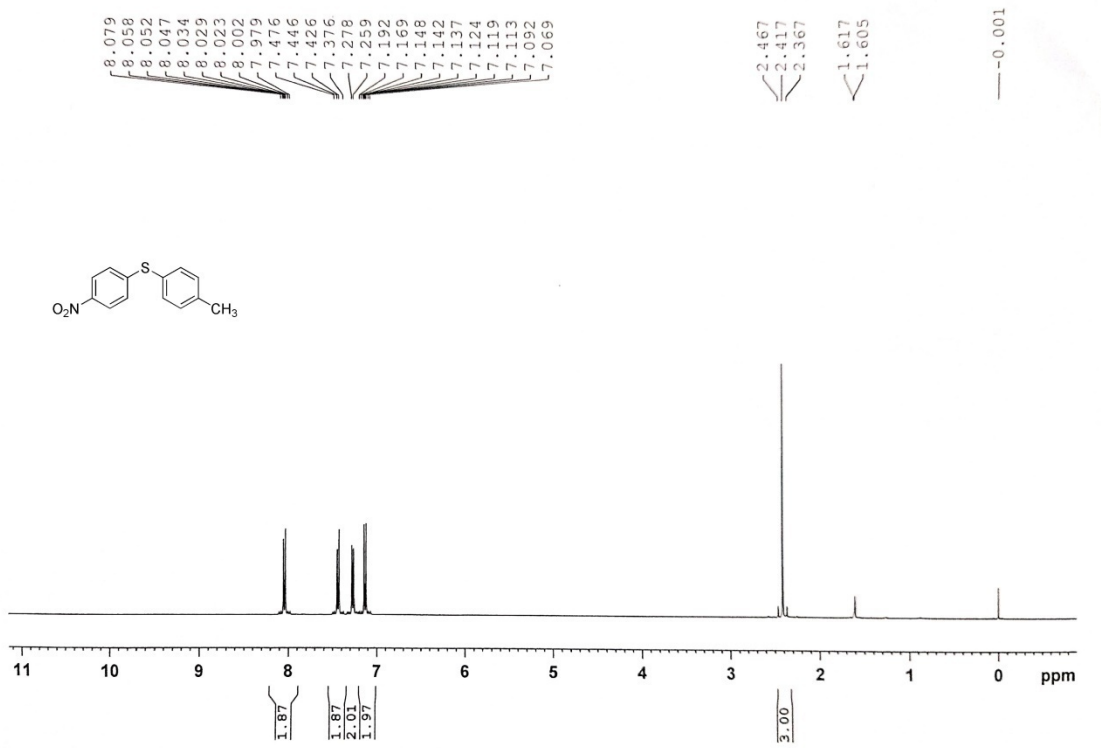
8.079
8.058
8.052
8.047
8.034
8.029
8.023
8.002
7.979
7.476
7.446
7.426
7.376
7.278
7.259
7.192
7.169
7.148
7.142
7.137
7.124
7.119
7.113
7.092
7.069
2.467
2.417
2.367
1.617
1.605
0.001
O2N
S
CH3
11
10
9
8
7
6
5
4
3
2
1
0
ppm
1.87
1.87
2.01
1.97
3.00

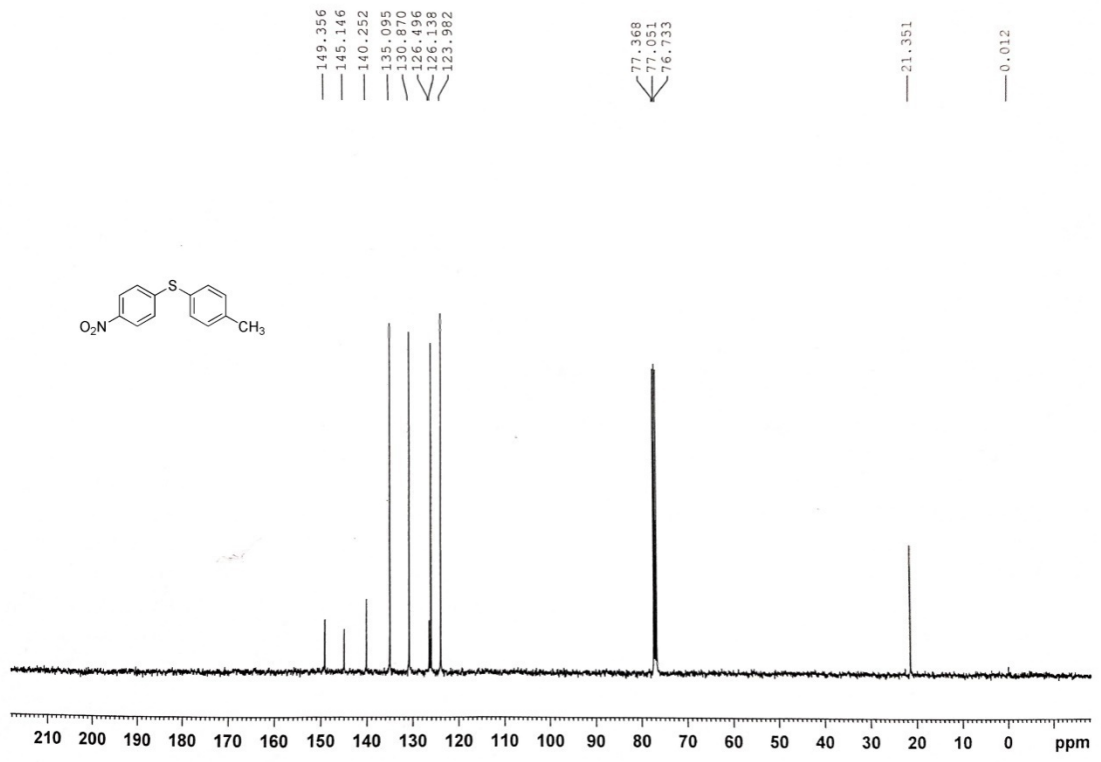
149.356
145.146
140.252
135.095
130.870
126.496
126.138
123.982
77.368
77.051
76.733
21.351
0.012
O2N
S
CH3
210
200
190
180
170
160
150
140
130
120
110
100
90
80
70
60
50
40
30
20
10
0
ppm

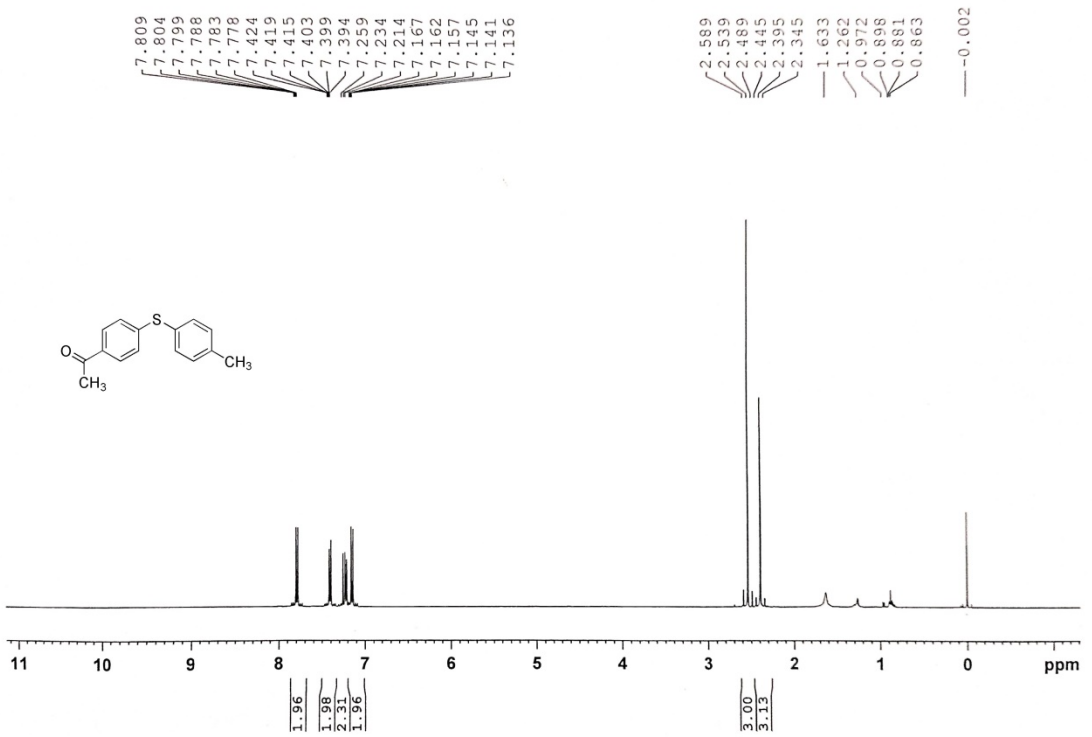
7.809
7.804
7.799
7.788
7.783
7.778
7.424
7.419
7.415
7.403
7.399
7.394
7.259
7.234
7.214
7.167
7.162
7.157
7.145
7.141
7.136
2.589
2.539
2.489
2.445
2.395
2.345
1.633
1.262
0.972
0.898
0.881
0.863
-0.002
O
S
CH3
CH3
11
10
9
8
7
6
5
4
3
2
1
0
ppm
1.96
1.98
2.31
1.96
3.00
3.13

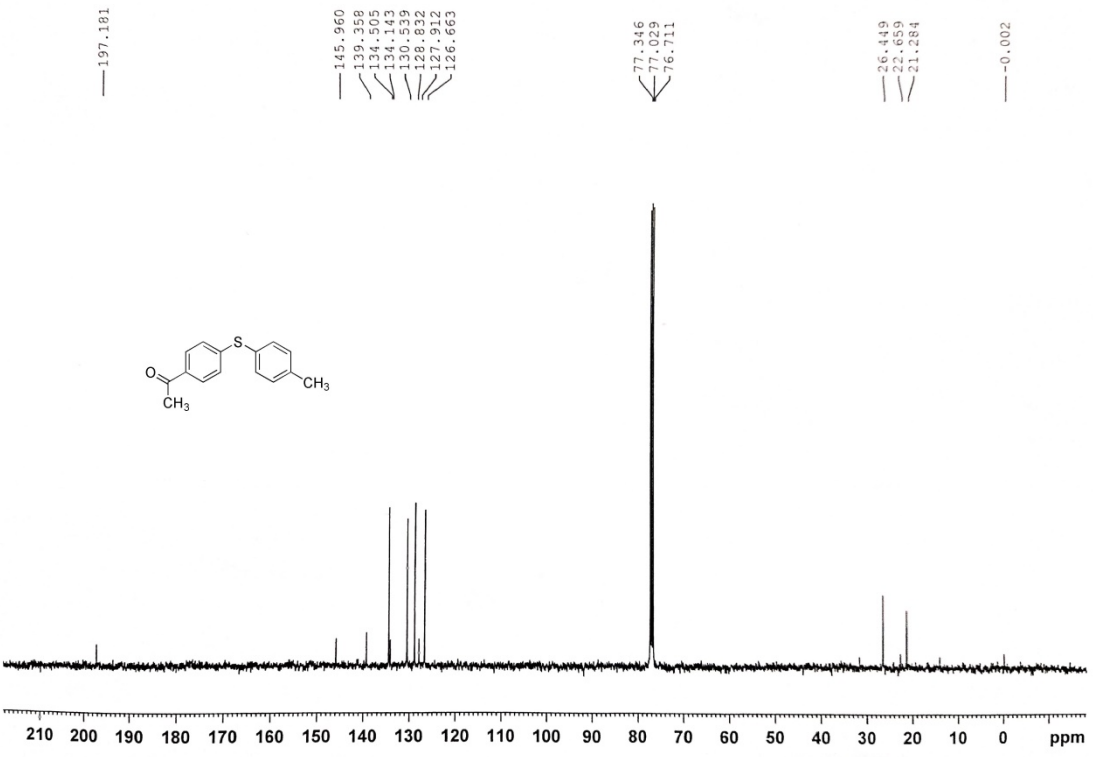
197.181
145.960
139.358
134.505
134.143
130.539
128.832
127.912
126.663
77.346
77.029
76.711
26.449
22.659
21.284
-0.002
O
S
CH3
CH3
210
200
190
180
170
160
150
140
130
120
110
100
90
80
70
60
50
40
30
20
10
0
ppm

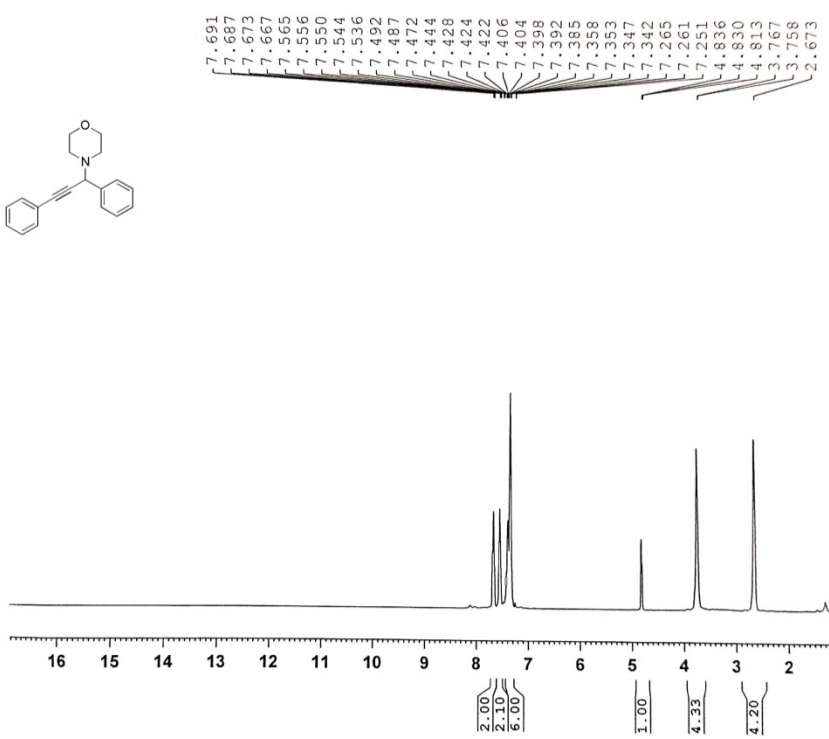
7.691
7.687
7.673
7.667
7.565
7.556
7.550
7.544
7.536
7.492
7.487
7.472
7.444
7.428
7.424
7.422
7.406
7.404
7.398
7.392
7.385
7.358
7.353
7.347
7.342
7.265
7.261
7.251
4.836
4.830
4.813
3.767
3.758
2.673
16 15 14 13 12 11 10 9 8 7 6 5 4 3 2 1 0 -1 -2 ppm
2.00
2.10
6.00
1.00
4.33
4.20

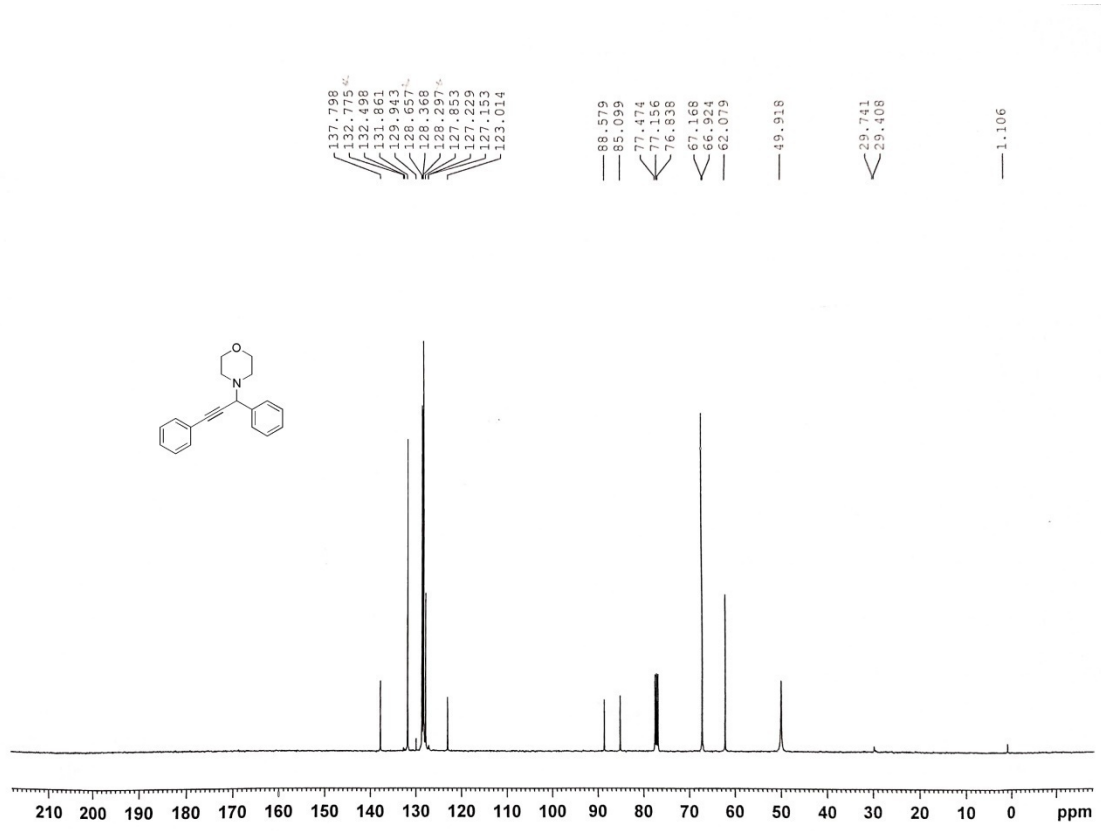
137.798
132.775
132.498
131.861
129.943
128.657
128.368
128.297
127.853
127.229
127.153
123.014
88.579
85.099
77.474
77.156
76.838
67.168
66.924
62.079
49.918
29.741
29.408
1.106
210 200 190 180 170 160 150 140 130 120 110 100 90 80 70 60 50 40 30 20 10 0 ppm

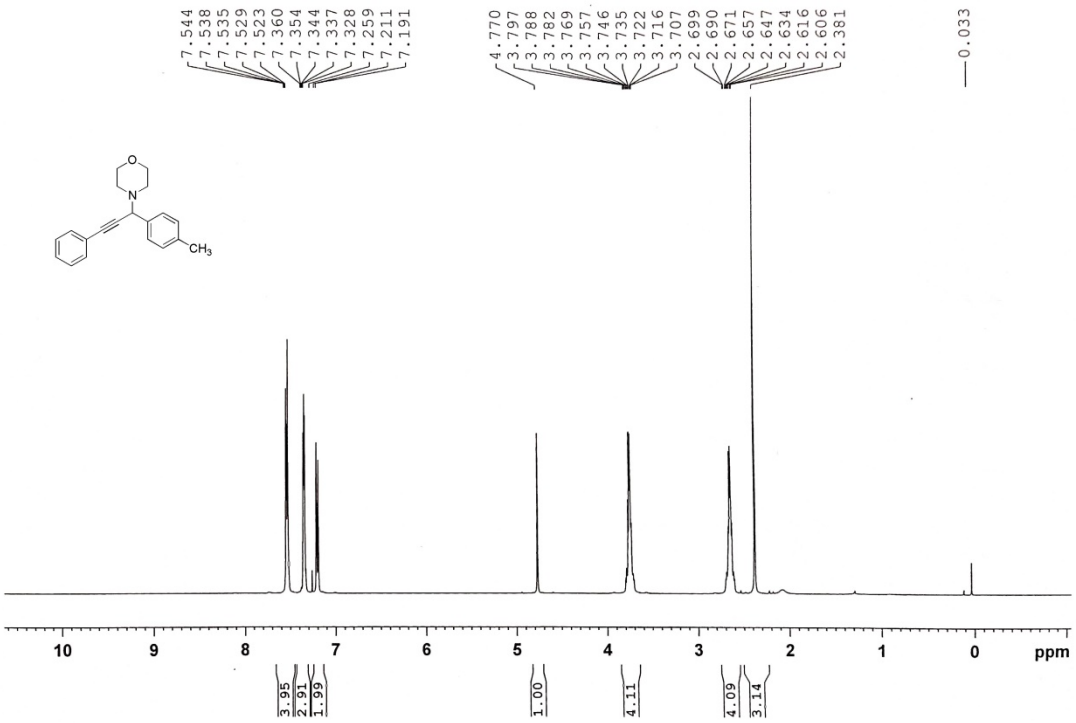
7.544
7.538
7.535
7.529
7.523
7.360
7.354
7.344
7.337
7.328
7.259
7.211
7.191
4.770
3.797
3.788
3.782
3.769
3.757
3.746
3.735
3.722
3.716
3.707
2.699
2.690
2.671
2.657
2.647
2.634
2.616
2.606
2.381
0.033
CH3
10
9
8
7
6
5
4
3
2
1
0
ppm
3.95
2.91
1.99
1.00
4.11
4.09
3.14

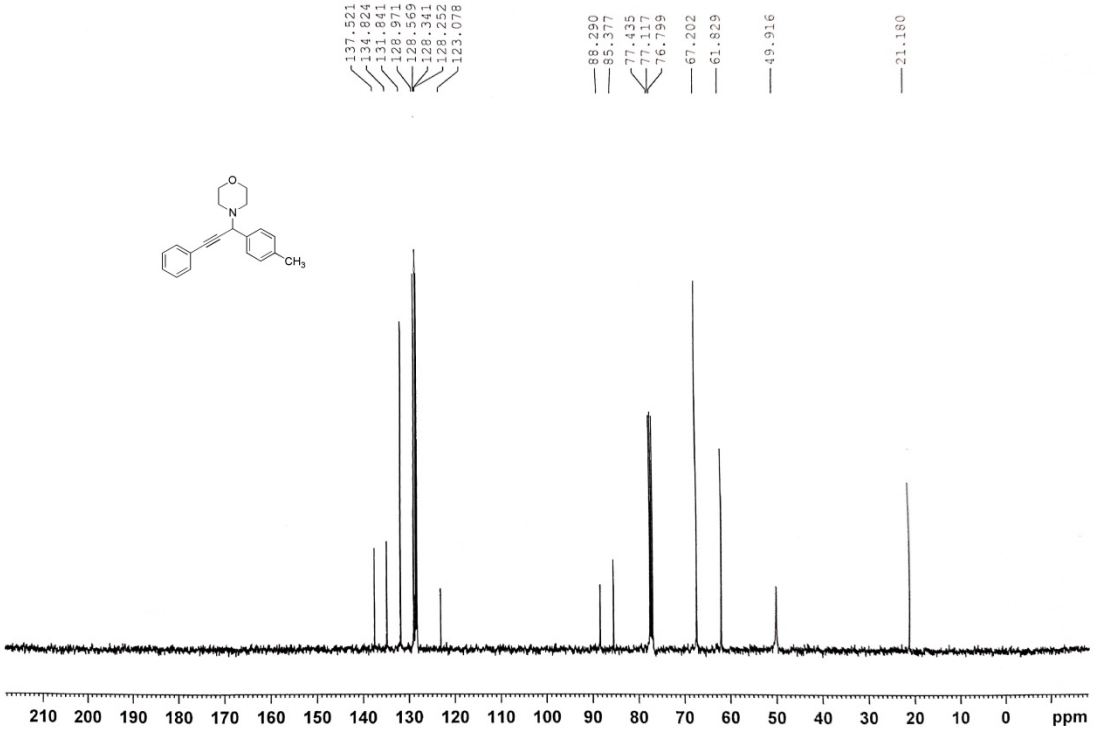
137.521
134.824
131.841
128.971
128.569
128.341
128.252
123.078
88.290
85.377
77.435
77.117
76.799
67.202
61.829
49.916
21.180
CH3
210
200
190
180
170
160
150
140
130
120
110
100
90
80
70
60
50
40
30
20
10
0
ppm

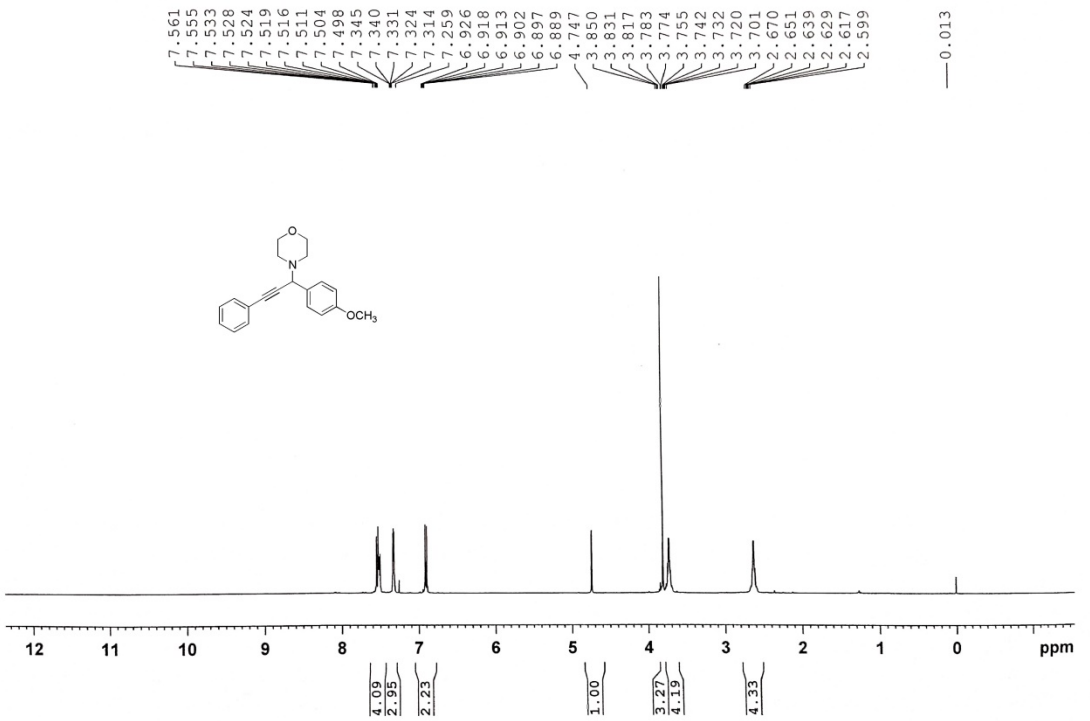
7.561
7.555
7.533
7.528
7.524
7.519
7.516
7.511
7.504
7.498
7.345
7.340
7.331
7.324
7.314
7.259
6.926
6.918
6.913
6.902
6.897
6.889
4.747
3.850
3.831
3.817
3.783
3.774
3.755
3.742
3.732
3.720
3.701
2.670
2.651
2.639
2.629
2.617
2.599
0.013
OCH3
12 11 10 9 8 7 6 5 4 3 2 1 0 ppm
4.09
2.95
2.23
1.00
3.27
4.19
4.33

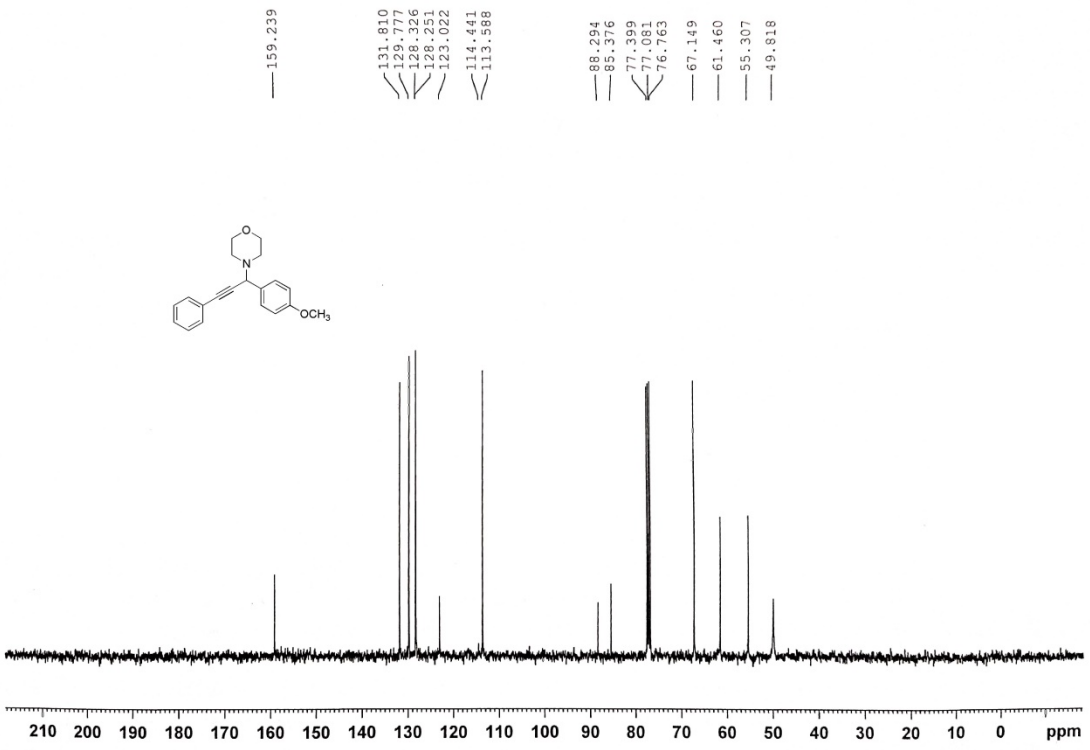
159.239
131.810
129.777
128.326
128.251
123.022
114.441
113.588
88.294
85.376
77.399
77.081
76.763
67.149
61.460
55.307
49.818
OCH3
210 200 190 180 170 160 150 140 130 120 110 100 90 80 70 60 50 40 30 20 10 0 ppm

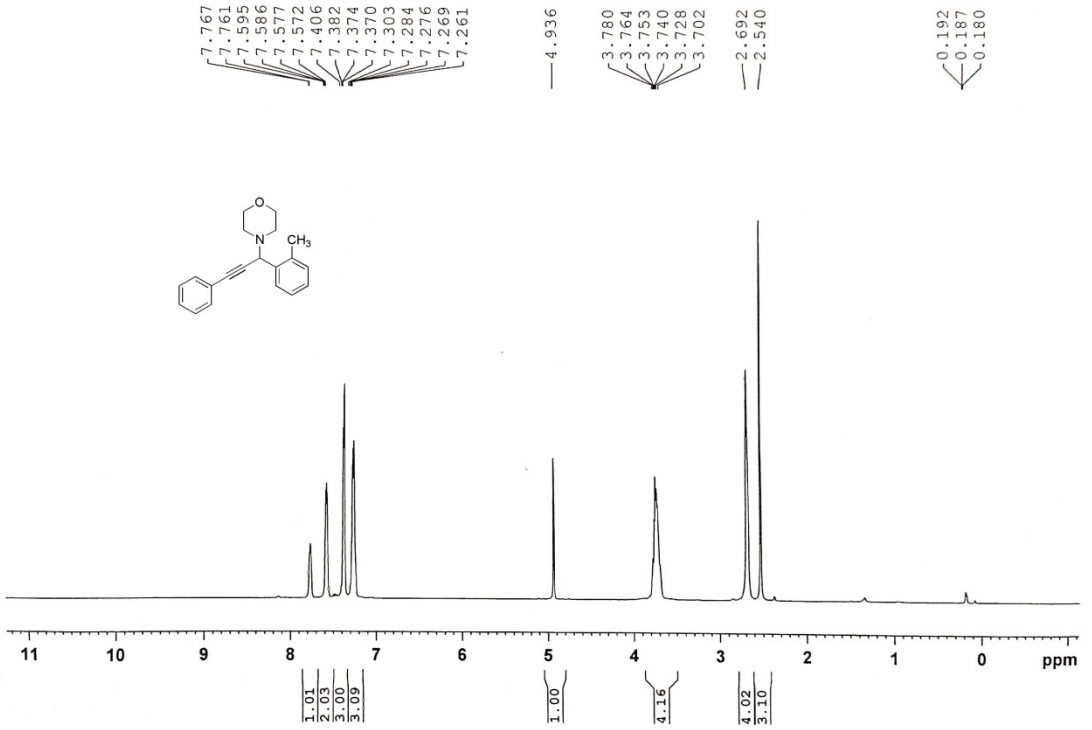
7.767
7.761
7.595
7.586
7.577
7.572
7.406
7.382
7.374
7.370
7.303
7.284
7.276
7.269
7.261
4.936
3.780
3.764
3.753
3.740
3.728
3.702
2.692
2.540
0.192
0.187
0.180
O
N
CH3
11 10 9 8 7 6 5 4 3 2 1 0 ppm
1.01
2.03
3.00
3.09
1.00
4.16
4.02
3.10

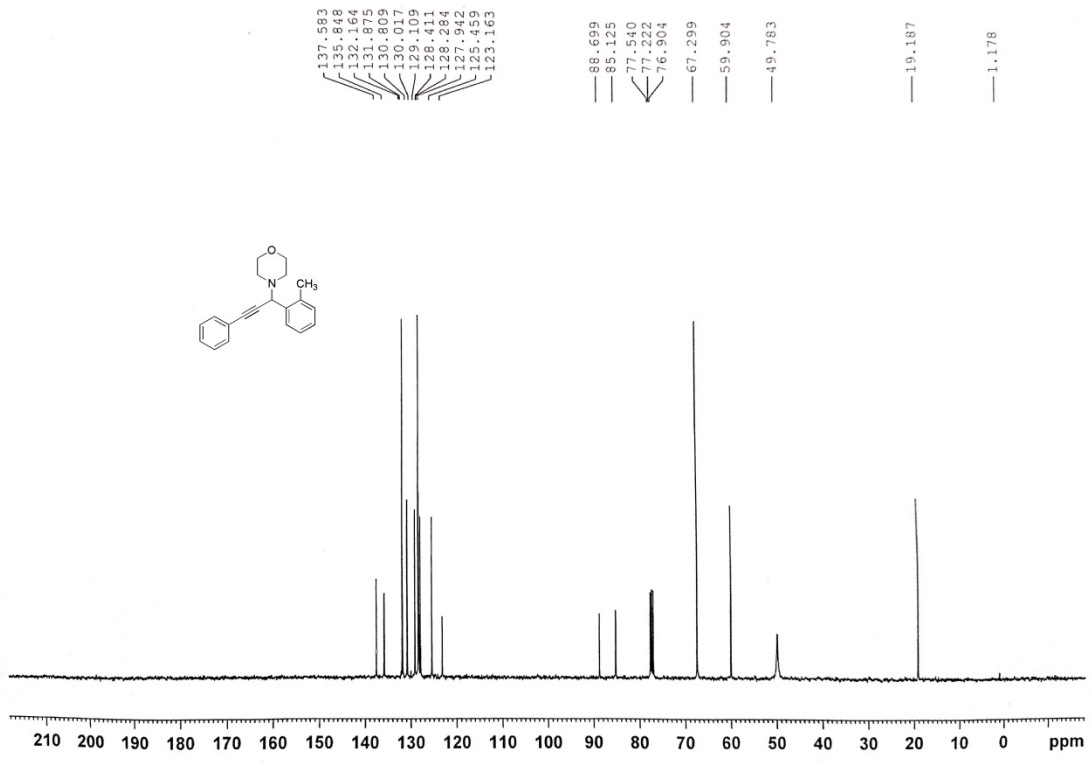
137.583
135.848
132.164
131.875
130.809
130.017
129.109
128.411
128.284
127.942
125.459
123.163
88.699
85.125
77.540
77.222
76.904
67.299
59.904
49.783
19.187
1.178
O
N
CH3
210 200 190 180 170 160 150 140 130 120 110 100 90 80 70 60 50 40 30 20 10 0 ppm

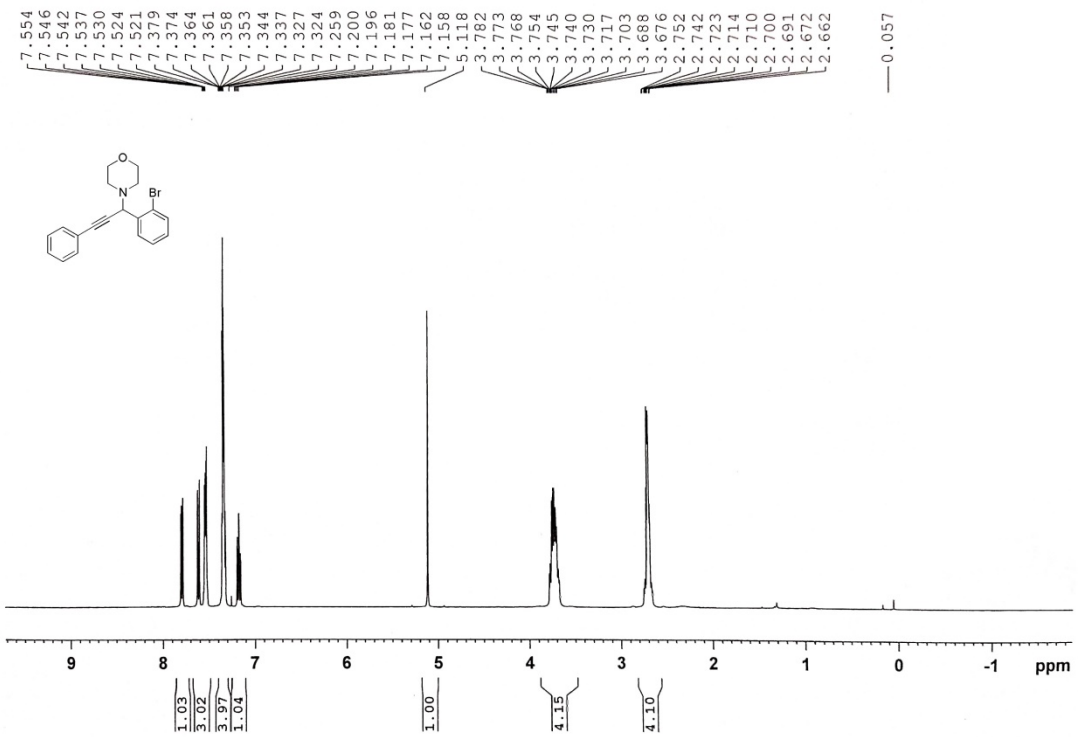
7.554
7.546
7.542
7.537
7.530
7.524
7.521
7.379
7.374
7.364
7.361
7.358
7.353
7.344
7.337
7.327
7.324
7.259
7.200
7.196
7.181
7.177
7.162
7.158
5.118
3.782
3.773
3.768
3.754
3.745
3.740
3.730
3.717
3.703
3.688
3.676
2.752
2.742
2.723
2.714
2.710
2.700
2.691
2.672
2.662
0.057
Br
9
8
7
6
5
4
3
2
1
0
-1
ppm
1.03
3.02
3.97
1.04
1.00
4.15
4.10

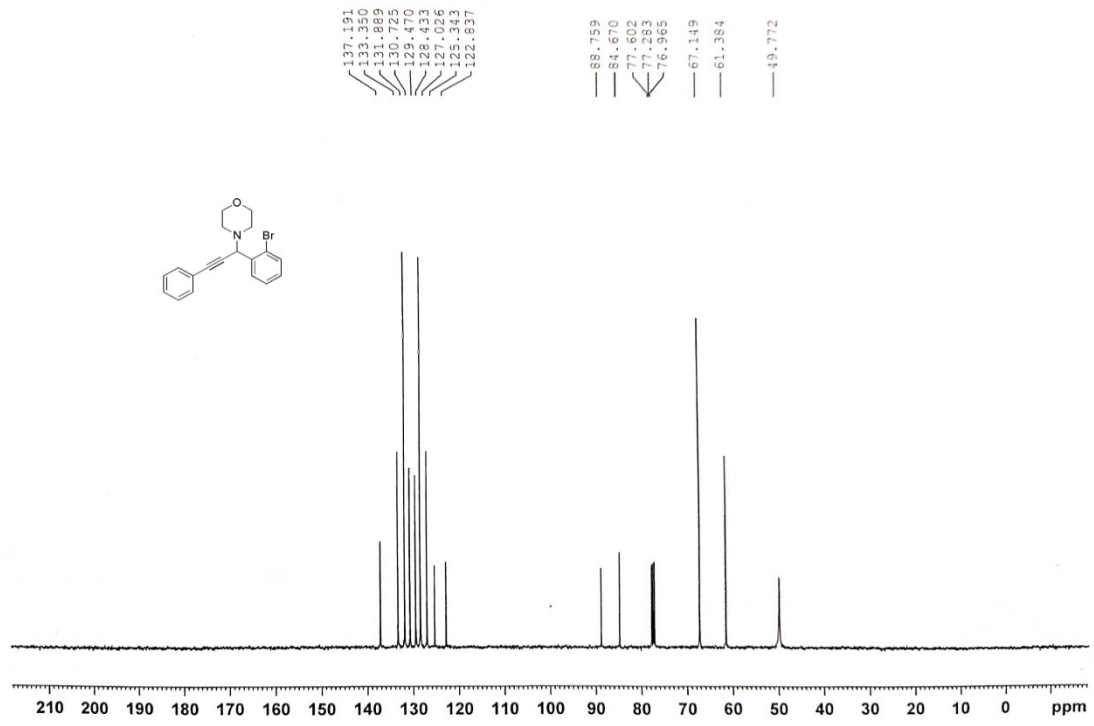
137.191
133.350
131.889
130.725
129.470
128.433
127.026
125.343
122.837
88.759
84.670
77.602
77.283
76.965
67.149
61.384
49.772
Br
210
200
190
180
170
160
150
140
130
120
110
100
90
80
70
60
50
40
30
20
10
0
ppm

## 6. Methods of In Silico Investigation and Computational Findings:

### Density functional theory (DFT)

The compounds 3a-h and 4a-e were optimized structurally using the Gaussian (G16) suite. To search for the minimized energy, the DFT model of restricted Becke's three parameters exchange potential and Lee-Yang-Parr correlation functional (RB3LYP) method was used along with the 6-311++G(d,p) basis set. The energy values and dipole moments of all molecules were calculated and are shown in Table 7.

### Molecular Docking Method:

In order to reveal the binding modes of the molecules, molecular docking studies were carried out as a significant tool for computer-assisted drug design using Autodock Vina software. The Gaussian-optimized output files of the ligands (3a-h and 4a-e) were prepared in pdbqt format using Open Babel software. The three-dimensional crystal structure of human pancreatic α-amylase (PDB ID: 4W93) and α-glucosidase (PDB ID: 5ZCC) was retrieved from the Research Collaboratory for Structural Bioinformatics-Protein Data Bank (RCSB–PDB) (http://www.rcsb.org/) and used as target enzymes. Before docking, all bound waters, ligands, and co-factors were removed from the receptors. Polar hydrogens were added geometrically during the receptor preparation, and the pdbqt file was saved on assigning Kollman's charges. Similarly, gasteiger charges were applied to the ligands. The grid box parameters; α-amylase: 50×50×50 size, -12.083, 3.406, -25.838 coordinates, α-glucosidase: 40×40×40 size, 5.184, 49.073, 73.866 coordinates. Other docking parameters were kept at the default level. The output files (protein-ligand complex) were analyzed using Discovery Studio Visualizer (v20.1.0.19295).

### Molecular dynamics (MD) simulation:

In this study, MD simulations were performed using GROMACS software (https://www.gromacs.org/) on selected docked complexes, using the CHARMM36 force field[54] for protein targets. *gmxgrep* command was used to extract the ligands from the complex, and then topology was generated using the CHARMM General Force Field (CGenFF) server,[55,56] followed by complex preparation within a 1 $nm^3$ cubic box filled with TIP3P water. The electroneutrality of the solvated system was maintained via the subsequent addition of sodium or chloride ions. The energy of the system was minimized and equilibrated using NPT and NVT ensembles for 100 ps at 310 K before a 10 ns MD simulation with 2 fs integration. After simulation, the analysis, such as RMSD, RMSF, Rg, SASA, and hydrogen bonds, was done by GROMACS modules of *gmxrms, gmxrmsf, gmx gyrate, gmxsasa,* and *gmxhbond*.

### Pharmacokinetic properties:

The SwissADME web server (http://www.swissadme.ch/) was used to examine the ADME profiles (Absorption, Distribution, Metabolism, and Excretion) of various compounds. The tool calculated physical descriptors, such as H-bond donors and acceptors and topological polar surface area (TPSA), for all compounds. In contrast, the OSIRIS property explorer (http://www.organic-

chemistry.org/prog/peo/) was used to calculate toxicological parameters. This program predicts the overall toxicity of a molecule by indicating fragment-based characteristics of mutagenic, tumorigenic, and irritant properties.

**7. Data of In Silico Investigation and Computational Findings:**

**Table 7:** Calculated energy values of the compounds using RB3LYP/6-311++G (d, p) basis set

| Compound | $E_{HOMO}$ (eV) | $E_{LUMO}$ (eV) | Band gap (eV) | Dipole Moment (Debye) |
|---|---|---|---|---|
| 3a | -5.68 | -0.96 | 4.71 | 0.98 |
| 3b | -5.96 | -0.99 | 4.97 | 1.93 |
| 3c | -5.88 | -0.85 | 5.02 | 2.85 |
| 3d | -5.99 | -1.03 | 4.97 | 3.91 |
| 3e | -6.04 | -0.96 | 5.08 | 1.17 |
| 3f | -6.71 | -2.93 | 3.78 | 5.07 |
| 3g | -6.63 | -2.71 | 3.92 | 6.85 |
| 3h | -6.23 | -1.77 | 4.46 | 5.81 |
| 4a | -6.06 | -1.29 | 4.77 | 1.67 |
| 4b | -5.79 | -1.25 | 4.53 | 1.79 |
| 4c | -5.97 | -1.22 | 4.75 | 2.12 |
| 4d | -6.01 | -1.23 | 4.79 | 1.56 |
| 4e | -6.15 | -1.24 | 4.91 | 1.58 |

**8. Methods of Biological Evaluation of the Synthesized Compound in Antioxidant and Antidiabetic Models**

**DPPH assay:**

DPPH assay was done to evaluate the free radical scavenging activity of the samples. Different concentrations of sample solution of 2 mL (10-100 µg/mL) in methanol were mixed into 1 mL of DPPH (0.3 mM) solution. The mixtures were stored in a dark area for 30 min and the absorbance was taken at 517 nm against blank. The positive control was ascorbic acid. The percentage of DPPH• scavenging activity was calculated by using the following equation:

% Scavenging of DPPH• = $[(A_0 - A1)/A_0] \times 100$,

$\mathbf{A_0}$ = absorbance of the control and **A1**= absorbance of the test samples. After determining the

% scavenging of DPPH• of the different concentrations, the $IC_{50}$ values were determined for the ascorbic acid and samples.

**α-Amylase Inhibitory Assay:**

The α-amylase inhibitory assay was measured by adding 25 ml sample solution (100-400 µg/mL), 50 µL of α-amylase (10 µ/mL) solution in phosphate buffer (pH 6.9), and 50 µL of starch solution (0.05%). The addition of 25µL of HCL (1M) was done to stop the reaction and further addition of 100 mL of iodine-potassium iodide solution. The final solution was incubated for 10 min at 37 °C. The absorbance of the solution was recorded at 630 nm. Acarbose was used as a positive control. The following formula was used to calculate the α-amylase inhibitory activity.

% Inhibitory activity = $[(A_0 - A1)/A_0] \times 100$,

$A_0$ = absorbance of the control and A1 = absorbance of the test samples. After determining the α-amylase inhibitory activity of the different concentrations, the $IC_{50}$ values were determined for the acarbose and samples.

**In-vitro antidiabetic activity**

**α-amylase inhibition assay**

The in-vitro antidiabetic potential was examined by using the α-amylase inhibition assay protocol.[59] Firstly, a serial dilution of the sample or standard (Acarbose) was prepared at 100 to 1000 µg/mL concentrations, using a phosphate buffer (pH 6.9, 0.06 M NaCl). A 500 µL aliquot of the sample was then transferred to a test tube, followed by the addition of 500 µL of α-amylase solution (13 U/mL). This mixture was incubated at 37 ℃ for 30 minutes. Then the 500 µL of 1% starch solution was added to it and further incubated for 20 min at 37℃. Lastly, 1mL of 3,5-dinitro salicylic acid was added to stop the reaction in a mixture. Lastly, the absorbance was measured at 500 nm. The test was carried out in triplicate. The half maximal inhibitory concentration ($IC_{50}$) was determined by using the percent inhibiting equation:

% Inhibitory activity = $[(A_0 – A_1)/ A_0] \times 100$, where $A_0$ and $A_1$ are absorbance of the control and sample respectively.

**α-glucosidase inhibition assay**

The α-glucosidase inhibition assay was carried out by a previously published method.[60] For this assay, 250 µL of potassium phosphate buffer (pH: 7.4, 100 mM), 150 µL of 4-nitrophenyl-αD-glucopyranoside (5 mM), 50 µL of standard or sample, and 150 µL of α-glucosidase were mixed and then incubated at 37 ℃ for 30 min. Then 600 µL of sodium bicarbonate (200 mM) was added to stop the reaction, and finally, the absorbance was measured at 400 nm. The percent inhibition was calculated by using the equation,

% Inhibition activity = $[(A_0 – A_1)/A_0] \times 100$; where $A_0$ = Absorbance of the control and $A_1$= Absorbance of the sample or standard.

**In-vivo antidiabetic assay**

**Animals for in-vivo studies**

For the anti-diabetic study, we used 40 Wistar Albino strain male adult rats that were in good health and weighed between 150 and 300 g. We bought them from Chakraborty Enterprise, an authorized dealer in Kolkata, India (Regd. No. 1443/PO/Bt/s/11/CPCSEA). The animals were kept under standard conditions (20 ± 2 °C, 50 ± 15% relative humidity, and a 12-hour light-dark cycle) in polypropylene cages (Tarsons, India) with bedding made of paddy husk. Rats had full access to water and standard food. The study received approval from the University of North Bengal's Institutional Animal Ethical Committee (IAEC) of the Committee for the Purpose of Control and Supervision of Experiments on Animals (CPCSEA) in West Bengal, India. All animal procedures were performed in accordance with the Guidelines for Care and Use of Laboratory Animals of the University of North

Bengal and approved by the Animal Ethics Committee of the University of North Bengal (IAEC/NBU/2022/35).

**Acute toxicities studies in rat**

The SR acute oral toxicity was tested in male Wister albino rats as per Organisation for Economic Cooperation and Development (OECD) Guideline 423. There were two groups of three rats in the experiment. As the control group, Group I received distilled water. Group II received SR (2,000 mg/kg) orally once. Following administration, every four hours for fourteen days, each animal was carefully checked for behavioural anomalies and general toxicity signs. The data on fatalities, body weight, and food intake were recorded.

**Oral glucose tolerance test (OGTT)**

In a rat model, we assessed the hypoglycaemic effects of methanolic extract by modifying the Reza et.al model.[61] There were four groups of six rats each in the experiment. The control group of rats received only distilled water (10 mL/kg b.w.), whereas the standard group of rats received metformin (70 mg/kg b.w.). 200 and 400 mg/kg b.w. doses of SR were administered to two distinct groups. All animals were starved for a whole night before the assay. Following an oral administration of the test sample and a 30 minutes rest time for the animals, we measured the fasting blood glucose level. Then each group was given an oral glucose solution (2 g/kg b.w.). After that, the glucose was administered, and we took blood from the rat's tail vein at 0, 30, 60, and 120 minutes. Lastly, we measured the blood glucose levels using an Accu-Check electronic glucometer.

**Type 2 diabetes induction**

The laboratory animals that had starved overnight were given 60 mg/kg body weight of streptozotocin (STZ) diluted in 0.1 M citrate buffer (pH 4.5) prepared with sterile water intraperitoneally (i.p.). We then gave them 100 mg/kg of nicotinamide 15 minutes later. After seven days, we chose rats with blood glucose levels greater than 200 mg/dL as type 2 diabetic rats for the study.

**Experimental design**

The animals were separated into five groups, each consisting of six individuals (n = 6).

**Group I**: Healthy control rats were administered distilled water (2 mL/kg, p.o.) daily for 28 days.

**Group II**: Diabetic control rats were given distilled water (2 mL/kg, p.o.) daily for 28 days.

**Group III**: Diabetic rats treated with SR (200 mg/kg, p.o.) daily for 28 days.

**Group IV**: Diabetic rats treated with SR (400 mg/kg, p.o.) daily for 28 days.

**Group V**: Diabetic rats were administered the standard drug Metformin (70 mg/kg, p.o.) daily for 28 days.

The treatments were carried out continuously for 28 days. Blood samples were collected from the tail vein on days 1, 7, 14, 21, and 28 to measure fasting blood glucose levels using a single-touch glucometer. All animals, including the healthy control group, fasted on these days to record body weight measurements.[60,62]

**Assessment of serum parameters**

On the 28th day, all animals were sacrificed to evaluate the effects of the methanolic extract administered to diabetic rats. The comparison included diabetic rats treated with the extracts, diabetic control rats, healthy normal animals, and the standard metformin-treated group. Various serum parameters were analysed, such as alkaline phosphatase (ALP), serum amylase, Serum Glutamic Pyruvic Transaminase (SGPT), Serum Glutamic Oxaloacetic Transaminase (SGOT), blood urea levels, and lipid profiles. These measurements were conducted using a standard enzyme-linked immunosorbent assay (ELISA) kit, following the protocol specified in the kit.

**Assessment of oxidative stress markers in liver tissues**

**Preparation of liver homogenate**

To evaluate oxidative stress in the liver, a 10% liver homogenate was prepared per the previously described protocol.[63] Specifically, 1 g of liver tissue was homogenized in 10 mL of cold phosphate buffer (pH 7.4) at 4 °C. The homogenate was centrifuged at 4 °C for 10 minutes at 12000 rpm. The supernatant obtained after centrifugation was used for the analysis of oxidative stress markers.

**Determination of lipid peroxidation**

Liver malondialdehyde (MDA) levels were measured using the standard protocol to assess liver peroxidation. Lipid peroxidation in the liver was determined calorimetrically by measuring thiobarbituric acid reactive substances (TBARS). The absorbance of the resulting clear supernatant was measured at 535 nm against a blank using a SPECTRO star Nano UV/vis plate reader (BMG LABTECH, Germany).

**Determination of catalase**

Catalase (CAT) activity was assessed using the previously established method. Absorbance changes were measured after 1 minute at 240 nm using a UV–VIS spectrophotometer (UV-1780, Shimadzu, Japan). One unit of CAT activity was defined as a 0.01 change in absorbance per minute.

**Histopathological studies**

A 10% formalin solution was used to preserve parts of the liver, kidney, and heart for histological examination. After being sectioned with a microtome, the paraffin-embedded tissues were stained with haematoxylin and eosin. The stained sections were subsequently seen at 40 × magnification using a Zeiss light microscope to assess the study's micro-level impacts on cells. The tissue sections have been taken to identify and evaluate damage to the related organs.[63]

**9. Synthesis and Characterization of CoFeLDH:**

The starting materials used in the present work were cobalt chloride ($CoCl_2.6H_2O$, Aldrich) and iron (III) chloride ($FeCl_3.6H_2O$, Aldrich) for the cobalt and iron precursors, respectively. Sodium hydroxide (50% w/w NaOH solution, Alfa Aeser) and sodium carbonate ($Na_2CO_3$, Fisher Chemicals) were used as precipitating agents for the formation of layer double hydroxides. Pure deionized water (18 MΩ/cm as obtained from Millipore Milli-Q) was used throughout this work. 21CoFeC-LDH [$Co_4Fe_2(OH)_{12}CO_3.3H_2O$] was prepared directly from the mixed metal ion precursor. For the synthesis of this LDH, 40 mmol of $CoCl_2.6H_2O$ and 20 mmol of $FeCl_3.6H_2O$ were dissolved in 100 mL of water

in a 250 mL round bottom flask. 50% w/w NaOH solution (180 mmole) was added dropwise with continuous stirring to the metal ion solution. 10 mmole of sodium carbonate was dissolved in 5 ml water and added to the above solution. The precipitate was formed and aged overnight in an oil bath at about 100 $^{o}$C with continuous refluxing and stirring. The precipitate was separated by centrifuge and washed several times with deionized water. It was dried in a vacuum over molecular sieves for several days to obtain the LDH for further analysis and characterization. The samples are calcined in the presence of air, He, and $H_2$ to obtain the metal/metal oxide and metal/metal nanocomposites. Phase analysis of the as-synthesized LDH powders as well as calcined samples in hydrogen and air was performed by powder X-ray diffraction (XRD) studies using a Siemens F-series instrument with Cu-Ka radiation (l = 0.15418 nm) and graphite-filter. The XRD data were collected at room temperature over the 2q range of 5 to 70$^{o}$ at a step size of 0.05$^{o}$ (2q) and a count time of 1s/step. Thermogravimetric (TG) analysis was recorded on a Perkin-Elmer TGA6 instrument using different reaction environments by flowing air, helium, and hydrogen (flow rate about 60 ml min$^{-1}$) at a heating rate of 10 $^{o}$C min$^{-1}$. XRD diffractograms were obtained to assess the crystal structure of CoFeLDH powder. Characteristic peaks for CoFeLDH powder were observed at 10°, 25°, 32°, 38°, 46°, 56°, and 65° and these angles indicated 111, 220, 311, 400, 511, and 440 (Figure 17), Bragg reflections, respectively. Peaks found at 56° and 65° indicate the presence of several interlayer anions. CoFeLDH was confirmed as a crystalline material from XRD analysis. Similar findings were reported for CoFeLDH (Sharmin et al. 2024).[19]

In addition, Fourier-transform infrared spectra (FTIR) were recorded using the KBr pellet technique on a Perkin-Elmer FTIR-1760X instrument; 40 scans were averaged to improve the signal-to-noise ratio within 400 to 4000 cm$^{-1}$ at a resolution of 4 cm$^{-1}$.

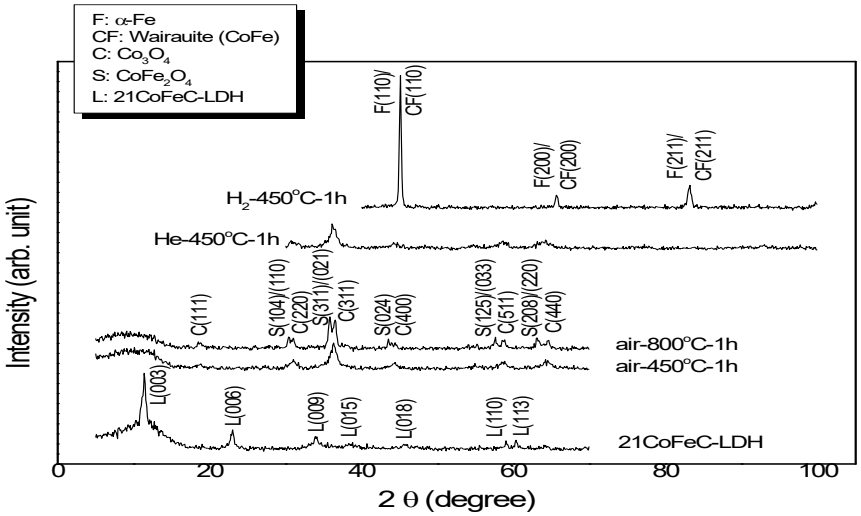

**Figure 17** XRD patterns of 21CoFeC-LDH and heat-treated samples in different medium.

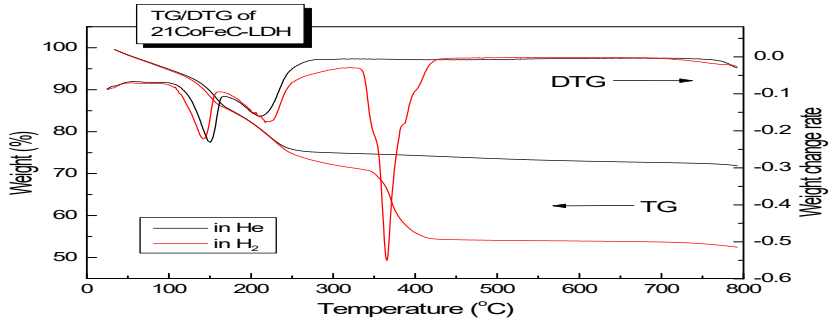


**Figure 18** TG/DTG of 21CoFeC-LDH in He and $H_2$.

The X-ray diffraction patterns of the as-prepared samples are shown in Figure 17, which confirm the formation of hydrotalcite-like structures. The XRD patterns give a series of (00l) peaks, such as (003), (006), and (009), appearing as broad symmetric lines at low 2q angle, corresponding to the basal spacing and higher order diffractions, and indicate that the samples consist of well crystallized single phase with small constituting crystallites. When 21CoFeC-LDH was heat treated under air and He at 450 °C, $Co_3O_4$ was formed. But at 800 °C in air, both $Co_3O_4$ and $CoFe_2O_4$ spinel were formed, and it is easy to distinguish these two phases as they have different XRD diffraction patterns. 21CoFeC-LDH has both the transition metals, so under reducing conditions in the presence of $H_2$, metal and metal alloys were formed. As both Fe and Wairauite (CoFe alloy) have the same crystalline structure, it is not possible to differentiate these two phases from XRD patterns. But there was no formation of Co metal under these conditions. Thermogravimetric analysis of the sample was carried out in He and $H_2$, to detect the decomposition as well as the reduction reaction of LDH during calculations. The TG curves together with the corresponding derivative TG curves (DTG) were recorded in He and $H_2$ of the LDH shown in Figure 18. The details of the thermal analysis results are summarized in Table 16(a) and Table 16(b). The thermal behaviour of hydrotalcite in an inert medium or air is generally characterized by two transitions: i) The first endothermic step at low temperature is due to the loss of interlayer water, without collapse of the structure; this step is reversible [x]. ii) The second endothermic peak at higher temperatures is due to the loss of the hydroxyl group from the brucite-like layer, as well as of the anions. In the presence of $H_2$, we have noticed an extra step of weight loss due to the reduction of metal ions to metal.

**Table 16(a):** Weight losses and products on heating LDH in inert atmospheres

| LDH system | Proposed formula | Residue in He | Calculated weight loss in He (%) | DTG $T_{max.}$ (°C) | Weight loss from TG in He (%) |
|---|---|---|---|---|---|
| 21CoFeC-LDH | $Co_4Fe_2(OH)_{12}CO_3.3H_2O$ | $Co_3O_4$, $CoFe_2O_4$ | 27.8 | 160, 215 | 27.2 |

**Table 16(b):** Weight losses and products on heating LDH in a hydrogen medium

| LDH system | Proposed formula | Residue in $H_2$ | Calculated weight loss in $H_2$ (%) | DTG $T_{max.}$ (°C) | Weight loss from TG in $H_2$ (%) |
|---|---|---|---|---|---|
| 21CoFeC-LDH | $Co_4Fe_2(OH)_{12}CO_3.3H_2O$ | Fe, CoFe | 47.8 | 146, 217, 369 | 47.6 |

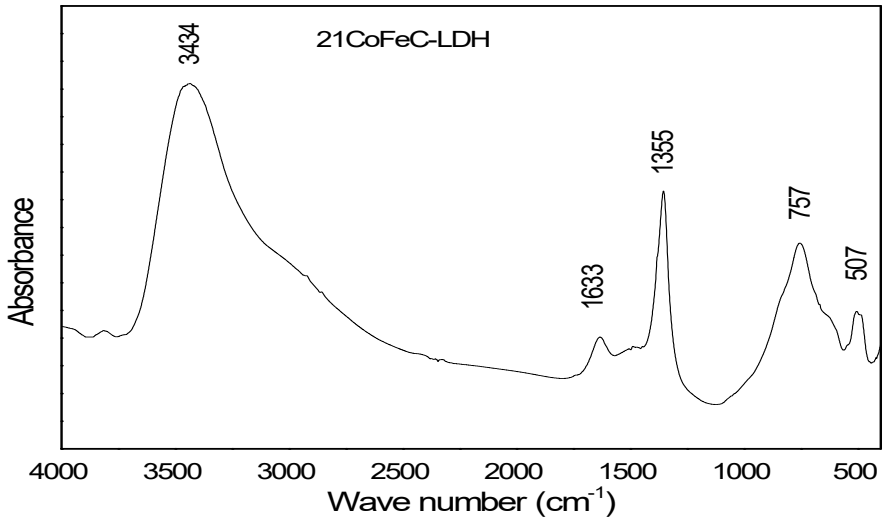


**Figure 19** FTIR spectra of 21CoFeC-LDH.

The FT-IR spectra (Figure 19) for the LDH sample showed a broad, intense band between 3400 to 3600 $cm^{-1}$ associated with a superposition of O-H stretching bands arising from metal-hydroxyl groups and hydrogen-bonded interlayer water molecules. A weak shoulder recorded in all of them around 3000 $cm^{-1}$ has been described as the O-H stretching mode of interlayer water molecules, hydrogen-bonded to interlayer carbonate anions [x]. The bending mode of water molecules is responsible for the weak band at about 1633 $cm^{-1}$. The rather sharp, intense band at about 1355 $cm^{-1}$ is due to mode $n^3$ antisymmetric stretching of interlayer carbonate, shifted from its position in free $CO_3^{2-}$ because of strong hydrogen bonding with hydroxy sheets and $H_2O$ molecule in the interlayer. Assignment for the bands at low-frequency regions from 1000 to 400 cm-1 has been reported by Kloprogge et al [x]. Based on comparison with their work, the bands at 507 and 757 $cm^{-1}$ can be assigned to translational modes of the hydroxyl groups mainly influenced by trivalent metals. The following simplified decomposition mechanism of LDH under air and $H_2$ was proposed according to the results of XRD, TG, and FTIR.

$$Co_4Fe_2(OH)_{12}CO_3.3H_2O \xrightarrow{Air} Co_3O_4 + CoFe_2O_4 \xrightarrow{H_2} 4\ Co + 2\ Fe$$